U-Pb Ages of Intrusive Rocks and $^{40}Ar/^{39}Ar$ Plateau Ages of Copper-Gold-Silver Mineralization Associated with Alkaline Intrusive Centres at Mount Polley and the Iron Mask Batholith, Southern and Central British Columbia

by J.M. Logan, M.G. Mihalynuk, T. Ullrich[1] and R.M. Friedman[1]

KEYWORDS: U-Pb zircon isotopic age, $^{40}Ar/^{39}Ar$ plateau cooling age, alkaline, porphyry copper-gold, mineralization, Afton, Ajax, Mount Polley, Northeast zone, hydrothermal breccia

INTRODUCTION

Porphyry deposits in British Columbia have produced more than $27 billion worth of copper and gold. They formed during two distinct periods in the development of the Cordillera: the first in the Late Triassic to Early Jurassic and the second in the Cretaceous to Eocene. Most porphyry production has come from the southern part of Quesnel Terrane, where two cycles of calcalkaline through alkaline magmatism are recognized in the Late Triassic and Early Jurassic. The reason for the *ca*. 10 Ma cycle of early calcalkaline and later alkaline volcanism, plutonism and mineralization is not fully resolved, but the same pattern repeated in the central and northern parts of the terrane suggest a feature fundamental to the Quesnel Arc genesis.

British Columbia alkaline porphyry deposits are associated with small, complex, either nepheline or leucite-normative intrusions and contain almost no quartz. The deposits comprise multiple, high-grade (0.5–1.0% Cu, 0.5–1.0 g/t Au) centres, each generally less than 150 million tonnes in size. Vein and stockwork development is insignificant and hydrothermal breccia-centred systems dominate. Mineralization is focused near the volcanic-plutonic interface, presumably as a result of late-stage magma devolatilization of highly oxidized (magnetite, hematite and anhydrite), primarily magmatic, high-salinity fluids. Late Triassic BC deposits are unique end-members of a continuum of porphyry deposits associated with calcalkaline, high-K calcalkaline or alkaline systems. Understanding the conditions of alkaline porphyry formation and the distinction between barren and fertile alkaline intrusions are important criteria for the evaluation of the Intermontane arc terranes and their economic potential in BC.

In 2004, the BC Ministry of Energy, Mines and Petroleum Resources, Abacus Mining and Exploration Corporation, Imperial Metals Corporation and Spectrum Gold Inc. (now NovaGold Resources) initiated a geoscience partnership agreement focused on refining the alkaline Cu-Au porphyry exploration model as it applies to the Iron Mask, Mount Polley and Galore Creek alkaline magmatic centres (Fig 1). Recent deposit and regional-scale geological mapping have established a better understanding of the stratigraphic and tectonic framework that hosts these alkaline Cu-Au mineral systems, their geochemistry and their ages of formation (Logan and Mihalynuk, 2005a, b; Bath and Logan, 2006; Logan and Bath, 2006).

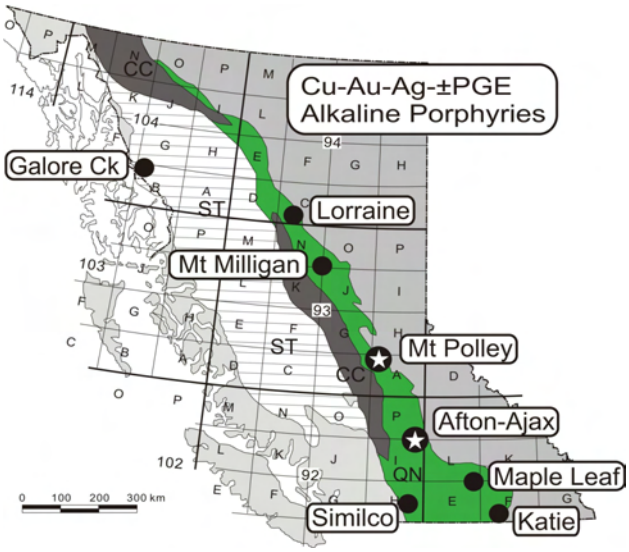

Figure 1. Location of BC Cu-Au-Ag±PGE alkaline porphyry deposits; green band indicates the Quesnel Terrane and the grey band indicates the Cache Creek Terrane. Abbreviation: ST, Stikine Terrane.

This report presents 17 new U-Pb and $^{40}Ar/^{39}Ar$ age determinations that have become available since the study began, for the Iron Mask batholith and the Mount Polley Cu-Au mine area. Data from Galore Creek and Copper Mountain will be presented separately.

GEOLOGICAL SETTING

The study area lies along the eastern margin of the Intermontane Belt close to its tectonic boundary with the Omineca Belt, in south-central BC (Fig 1). At this latitude, the Intermontane Belt is underlain mainly by Late Paleozoic to Early Mesozoic arc volcanic, plutonic and sedimentary rocks of the Quesnel Terrane. Farther west are coeval rocks of the oceanic Cache Creek Terrane. The southern Quesnel Terrane consists of an isotopically and

[1] *University of British Columbia, Vancouver, BC*

This publication is also available, free of charge, as colour digital files in Adobe Acrobat® PDF format from the BC Ministry of Energy, Mines and Petroleum Resources website at http://www.em.gov.bc.ca/Mining/Geolsurv/Publications/catalog/cat_fldwk.htm

geochemically primitive Late Triassic to Early Jurassic magmatic arc complex, which formed above an east-dipping subduction zone (Mortimer, 1987). The Cache Creek Terrane, with its Late Triassic (Paterson and Harakal, 1974; Ghent *et al.,* 1996) blueschist-facies rocks, represents the remnants of this subduction-accretionary complex (Travers, 1977; Mihalynuk *et al.,* 2004). Quesnellia is fault-bounded, juxtaposed on the west with Paleozoic and Mesozoic rocks of the Cache Creek Complex and on the east by Mesozoic to Paleozoic and older metasedimentary, metavolcanic and metaplutonic rocks of the pericratonic Kootenay 'terrane'. Slide Mountain Terrane rocks have been interpreted to represent the remnants of a Late Paleozoic marginal basin (Schiarizza, 1989; Roback *et al*., 1994), which separated Quesnellia from North America until its closure in the Early Jurassic. By Middle Jurassic time, Stikinia had collided with Quesnellia, resulting in the demise of the Cache Creek subduction zone (173 Ma) and the stitching of the boundary in the northern Cordillera by *ca.*172 Ma plutons (Mihalynuk *et al.,* 2004). At the same time, the Quesnellia, Slide Mountain, Barkerville and Cariboo subterranes were imbricated and thrust eastward onto the North American craton (Nixon *et al.,* 1993). Cretaceous intrusions, Tertiary volcanic rocks and feeder dikes of the Eocene Kamloops and Miocene Chilcotin groups are the youngest rocks in the region (Mathews, 1989).

Quesnel Arc magmatism and associated porphyry mineralization migrated eastward with time, beginning in the west, *ca.* 210 to 215 Ma, with the emplacement of plutons and the development of calcalkaline Cu-Mo±Au deposits at Highland Valley and Gibraltar. New data suggests that mineralization at Highland Valley postdates the intrusion of the Guichon batholith by up to 4 Ma (*see* Ash *et al*., 2007). East of Gibraltar, in the central axis of the arc, are alkaline intrusions and 205 Ma, Cu-Au mineralization at Mount Polley. A chain of similar deposits extends the length of the Intermontane Belt (Barr *et al.,* 1976; Fig 1). In the south, they are associated with the Iron Mask batholith (Afton, Ajax and Crescent) and Copper Mountain intrusive rocks (Copper Mountain, Ingerbelle) and to the north, with the Hogem batholith (Lorraine). Uplift and erosion of the fore arc produced sub-Jurassic unconformities as magmatism shifted east and culminated with the intrusion of calcalkaline composite plutons consisting of quartz monzodiorite (*ca.* 202 Ma) and granodiorite (193–195 Ma) phases (Schiarizza and Macauley, 2007) in the south (Takomkane, Thuya, Wild Horse and Pennask) and deposition of distal volcaniclastic and younger sedimentary rocks across the terrane. A temporally unrelated, *ca*.183 Ma syn-accretionary pulse of alkaline magmatism and Cu-Au mineralization is recognized at Mount Milligan, 275 km northwest of Mount Polley. Post-accretion plutons in the central Quesnel belt include a Middle Jurassic (*ca.* 163 Ma) alkali leucogranite associated with Cu-Mo mineralization at Gavin Lake, and the *ca*. 104 Ma, mid-Cretaceous Bayonne suite plutons associated with Mo mineralization at Boss Mountain deposit and the Anticlimax showing.

GEOCHRONOLOGY

First attempts at determining the ages of Cu-Au mineralization within the Iron Mask batholith by Cockfield (1948) and Northcote (1977) and at Mount Polley by Campbell (1978) and Bailey (1978) used stratigraphic and paleontological constraints. Subsequent K-Ar isotopic dating of intrusions and alteration assemblages associated with mineralization were reported by Preto *et al*. (1979) for the Iron Mask batholith and by Panteleyev *et al*. (1996) and Bailey and Archibald (1990) for various intrusions in the Mount Polley region. On the basis of the K-Ar age data and alkaline compositions, most of these intrusions were included in the Early and Middle Jurassic Copper Mountain suite by Woodsworth *et al*. (1991).

Prior to the widespread application of U-Pb techniques to date intrusions, the majority of the age data for Cordilleran porphyry systems consisted of K-Ar and Rb-Sr cooling or isotopic disturbance ages (R.L. Armstrong, UBC data file) rather than crystallization ages. In areas of protracted magmatism or subsequent thermal/hydrothermal overprinting, common in porphyry deposits, neither the K-Ar nor the Rb-Sr technique can provide a reliable crystallization age. Using the U-Pb age dating technique, Mortensen *et al*. (1995) was able to resolve two discrete episodes of alkaline magmatism associated with copper-gold mineralization in the Canadian Cordillera: 210 Ma to 200 Ma and 183 Ma. Armed with the revised time scale of Palfy *et al*. (2000), subsequent workers were able to determine that the older episode, including intrusive phases at the Iron Mask batholith (204 ±3 Ma) and at Mount Polley (204.7 ±3 Ma), falls entirely within the Late Triassic, while the younger episode is Early Jurassic in age. Our geochronological work was aimed at establishing a finer temporal resolution for magmatic-hydrothermal events at existing deposits, as well as evaluating whether compositionally similar intrusions in the belt are coeval with the important 204 Ma Cu-Au metallogenic event.

ANALYTICAL TECHNIQUES

All U-Pb and $^{40}Ar/^{39}Ar$ sample preparation and analytical work was conducted at the Pacific Centre for Isotopic and Geochemical Research (PCIGR) at the Department of Earth and Ocean Sciences, University of British Columbia. Analytical results determined by U-Pb methods are listed in Tables 1 and 2. Step-heating gas release plots for $^{40}Ar/^{39}Ar$ analyses and concordia plots for U-Pb analyses are shown in Figures 3, 6, 9 and 11.

U-Pb-Thermal Ionization Mass Spectrometry

Zircon was separated from samples using conventional crushing, grinding and Wilfley table techniques, followed by final concentration using heavy liquids and magnetic separations. For this study, coarse titanite was disaggregated directly from hand samples with no additional mineral separation necessary. Zircon fractions were selected on the basis of grain quality, size, magnetic susceptibility and morphology. All zircon fractions were air abraded prior to dissolution to minimize the effects of post-crystallization Pb loss, using the technique of Krogh (1982). Mineral fractions were dissolved in sub-boiled 48% HF and 14 M HNO_3 (ratio of ~10:1, respectively) in the presence of a mixed $^{233-235}U$–^{205}Pb tracer; zircons for 40 hours at 240°C in 300 µL PTFE or PFA microcapsules contained in high-pressure vessels (Parr™ acid digestion vessels with 125 mL PTFE liners) and titanite on a hotplate in 7 mL screw-top PFA beakers for at least 48 hours at ~130°C. Sample solutions were then dried to salts at ~130°C. Zircon residues were re-dissolved in ~100 µL of

sub-boiled 3.1 M HCl for 12 hours at 210°C in high-pressure vessels and titanite residues on a hotplate in ~1 mL of sub-boiled 6.2 M HCl in the same 7 mL screw-top PFA beakers for at least 24 hours at ~130°C. Titanite solutions were again dried to salts and were again re-dissolved on a hotplate, in the same beakers, in 1 mL of sub-boiled 3.1 M HCl at ~130°C for at least 24 hours. For single-grain zircon fractions E, F and G, sample JLO-05-6-27 3.1 M HCl was transferred to 7 mL PFA beakers, dried to a small droplet after the addition of 2 µL of 1 M H_3PO_4 and loaded directly on to Re filaments for analysis, as described below. For all other zircon and titanite fractions, the separation and purification of Pb and U employed ion exchange column techniques modified slightly from those described by Parrish *et al*. (1987). Lead and uranium were sequentially eluted into a single beaker; U from titanite solutions was purified by passing through columns a second time. Elutants were dried in 7 mL screw-top PFA beakers on a hotplate at ~120°C in the presence of 2 µL of ultra-pure 1 M phosphoric acid (H_3PO_4). Samples were then loaded on single, degassed zone refined Re filaments in 5 µL of a silica gel ($SiCl_4$) phosphoric acid emitter. Isotopic ratios were measured using a modified single collector VG-54R thermal ionization mass spectrometer equipped with an analogue Daly photomultiplier. Measurements were done in peak-switching mode on the Daly detector. Analytical blanks during the course of this study were <1 pg for U and for Pb in the range of 1 to 3 pg for no chemistry fractions and 2 to 10 pg for zircons passed through columns and titanite. Uranium fractionation was determined directly on individual runs using the $^{233\text{-}235}U$ tracer and Pb isotopic ratios were corrected for the fractionation of 0.32 to 0.37%/amu, based on replicate analyses of the NBS-982 Pb standard and the values recommended by Thirlwall (2000). Reported precisions for Pb/U and Pb/Pb dates were determined by numerically propagating all analytical uncertainties through the entire age calculation using the technique of Roddick (1987). Standard concordia diagrams were constructed and regression intercepts calculated with Isoplot v. 3.00 (Ludwig, 2003). Unless otherwise noted, all errors on interpreted ages are quoted at the 2σ level.

U-Pb thermal ionization mass spectrometry (TIMS) analytical results are presented in Table 1. Discussion of results in a geological context follow in these sections: 'Iron Mask', 'Mount Polley', 'Shiko Lake Stock', 'Woodjam Property' and 'Gavin Lake'.

Laser Ablation Inductively Coupled Plasma Mass Spectrometry

Laser ablation inductively coupled plasma mass spectrometry (LA-ICP-MS) dating has recently been established as a routine procedure at the PCIGR. Zircons are separated from their hostrocks using conventional mineral separation methods and sectioned in an epoxy grain mount along with grains of internationally accepted standard zircon (FC-1, a *ca*. 1100 Ma zircon standard), and brought to a very high polish. The grains are examined using a stage-mounted cathodoluminescence imaging set-up that makes it possible to detect the presence of altered zones or inherited cores within the zircon. The highest-quality portions of each grain, free of alteration, inclusion or cores, are selected for analysis. The surface of the mount is then washed for ~10 minutes with dilute nitric acid and rinsed in ultra-clean water. Analyses are carried out using a New Wave 213 nm Nd-YAG laser coupled to a Thermo Finnigan Element2 high-resolution ICP-MS. Ablation takes place within a New Wave 'Supercell' ablation chamber, which is designed to achieve very high efficiency entrainment of aerosols into the carrier gas. Helium is used as the carrier gas for all experiments and gas flow rates, and together with other parameters, such as torch position, are optimized prior to beginning a series of analyses. We typically use a 25 μm spot with 60% laser power, and do line scans rather than spot analyses in order to avoid within-run elemental fractions. Each analysis consists of a 7 second background measurement (laser off) followed by a ~28 second data acquisition period with the laser firing. A typical analytical session consists of four analyses of the standard zircon, followed by four analyses of unknown zircons, two standard analyses, four unknown analyses, etc. and finally four standard analyses. Data are reduced using the GLITTER software developed by the Geochemical Evolution and Metallogeny of Continents (GEMOC) group at Macquarrie University, which can subtract background measurements, propagate all analytical errors and calculate isotopic ratios and ages. This application generates a time-resolved record of each laser shot. Final ages for contiguous populations of relatively young (Phanerozoic) zircons are based on a weighted average of the calculated $^{206}Pb/^{238}U$ ages for 10 to 15 individual analyses. Interpretation and plotting of the analytical results employs Isoplot v. 3.00 software (Ludwig, 2003).

The LA-ICP-MS analytical results are presented in Table 2. A discussion of results in a geological context follow in these sections: 'Iron Mask', 'Mount Polley', 'Shiko Lake Stock', 'Woodjam Property' and 'Gavin Lake'.

Ar/Ar

Mineral separates were hand-picked, washed in nitric acid, rinsed in de-ionized water, dried, wrapped in aluminum foil and stacked in an irradiation capsule with similar-aged samples and neutron flux monitors (Fish Canyon tuff sanidine, 28.02 Ma; Renne *et al*., 1998). The samples were irradiated on February 15 to 17, 2006 at the McMaster Nuclear Reactor in Hamilton, Ontario, for 90 MWh, with a neutron flux of approximately 3 by 10^{16} neutrons/cm^2/s. Analyses (n = 57) of 19 neutron flux monitor positions produced errors of <0.5% in the J value.

The samples were analyzed at the Noble Gas Laboratory, Pacific Centre for Isotopic and Geochemical Research, The University of British Columbia, Vancouver. The mineral separates were step-heated at incrementally higher powers in the defocused beam of a 10 W CO_2 laser (New Wave Research MIR10) until fused. The gas evolved from each step was analyzed by a VG5400 mass spectrometer equipped with an ion-counting electron multiplier. All measurements were corrected for total system blank, mass spectrometer sensitivity, mass discrimination, radioactive decay during and subsequent to irradiation, as well as interfering Ar from atmospheric contamination and the irradiation of Ca, Cl and K (isotope production ratios: $[^{40}Ar/^{39}Ar]_K$=0.0302 ±0.00006; $[^{37}Ar/^{39}Ar]_{Ca}$=1416.4 ±0.5; $[^{36}Ar/^{39}Ar]_{Ca}$=0.3952 ±0.0004, Ca/K=1.83 ±0.01$[^{37}Ar_{Ca}/^{39}Ar_K]$).

The plateau and correlation ages were calculated using Isoplot v. 3.00 (Ludwig, 2003). Errors are quoted at the 2σ (95% confidence) level and are propagated from all sources except mass spectrometer sensitivity and age of the flux

TABLE 1. U-PB THERMAL IONIZATION MASS SPECTROMETRY (TIMS) ANALYTICAL DATA.

Fraction[1]	Wt (mg)	U[2] (ppm)	Pb*[3] (ppm)	$^{206}Pb/^{204}Pb$[4]	Pb[5] (pg)	Th/U[6]	Isotopic ratios (1σ, %)[7] $^{206}Pb/^{238}U$	$^{207}Pb/^{235}U$	$^{207}Pb/^{206}Pb$	Apparent ages (2σ, Ma)[7] $^{206}Pb/^{238}U$	$^{207}Pb/^{235}U$	$^{207}Pb/^{206}Pb$
JLO-04-2-14												
T1, 3	179	42	1.5	65	308	0.87	0.03103 (0.78)	0.2107 (3.3)	0.04925 (2.9)	197.0 (3.0)	194 (12)	160 (130/141)
T2, 5	214	41	1.4	65	370	0.67	0.03130 (1.1)	0.2169 (3.9)	0.05027 (3.3)	198.7 (4.4)	194 (14)	208 (144/158)
T3, 2	181	70	2.4	90	354	0.66	0.03154 (0.74)	0.2132 (2.7)	0.04901 (2.2)	200.2 (2.9)	196.2 (9.4)	148 (101/107)
JLO04-21-84												
A, 6	34	573	19.6	4457	8.0	0.97	0.02918 (0.11)	0.2009 (0.25)	0.04994 (0.20)	185.4 (0.4)	185.4 (0.4)	192.0 (9.4/9.5)
B, 7	27	899	42.6	6179	7.3	2.54	0.02959 (0.23)	0.2038 (0.37)	0.04994 (0.27)	188.0 (0.9)	188.3 (1.3)	192 (13)
C, 8	21	818	32.2	5035	6.4	1.55	0.02956 (0.10)	0.2035 (0.24)	0.04992 (0.19)	187.8 (0.4)	188.1 (0.8)	191.3 (8.9/9.0)
D, 10	9	674	19.3	1869	5.9	2.25	0.02938 (0.17)	0.2023 (0.54)	0.04994 (0.49)	186.7 (0.6)	187.1 (1.8)	192 (23)
E, 10	13	343	19.0	2149	3.9	3.41	0.03013 (0.19)	0.2073 (0.47)	0.04990 (0.43)	191.3 (0.7)	191.3 (1.6)	190 (20)
JLO04-24-111												
A, 3	4	1597	66.7	2656	4.8	1.40	0.03246 (0.20)	0.2266 (0.57)	0.05063 (0.54)	205.9 (0.8)	207.4 (2.2)	224 (25)
B, 7	7	1230	49.5	2927	6.0	1.25	0.03224 (0.10)	0.2239 (0.35)	0.05038 (0.31)	204.6 (0.4)	205.2 (1.3)	213 (14/15)
C, 11	5	1403	55.8	5303	2.7	1.19	0.03227 (0.15)	0.2246 (0.28)	0.05048 (0.24)	204.7 (0.6)	205.8 (1.1)	217 (11)
D, 14	6	1093	45.9	5904	2.3	1.43	0.03245 (0.10)	0.2267 (0.25)	0.05066 (0.21)	205.9 (0.4)	207.5 (0.9)	225.4 (9.7/9.8)
E, ~30	12	837	34.2	9533	2.2	1.31	0.03234 (0.14)	0.2260 (0.22)	0.05067 (0.18)	205.2 (0.6)	206.9 (0.8)	226.1 (8.5)
JLO-04-50-510												
B, 2	42	197	6.6	4478	3.7	0.49	0.03229 (0.09)	0.2238 (0.20)	0.05027 (0.15)	204.9 (0.4	204.9 (0.7)	207.3 (6.9/7.0)
D, 2	47	784	31.9	33080	2.2	1.31	0.03227 (0.09)	0.2239 (0.16)	0.05032 (0.09)	204.7 (0.4	205.1 (0.6)	209.7 (4.1/4.2)
E, 4	57	286	9.7	2793	11.5	0.52	0.03235 (0.10)	0.2230 (0.59)	0.04999 (0.55)	205.2 (0.4	204.4 (2.2)	195 (25/26)
MMI04-26-18												
A, 2	144	73	2.3	3147	6.3	0.38	0.03085 (0.10)	0.2126 (0.31)	0.04997 (0.26)	195.9 (0.4	195.7 (1.1)	194 (12)
B, 4	201	55	1.7	4231	5.0	0.41	0.03065 (0.09)	0.2115 (0.26)	0.05006 (0.21)	194.6 (0.4	194.9 (0.9)	198 (10)
D, 5	189	89	2.8	4657	6.8	0.40	0.03100 (0.31)	0.2136 (0.33)	0.04997 (0.31)	196.8 (1.2	196.5 (1.2)	194 (14/15)
E, 6	222	57	1.8	3585	6.7	0.44	0.03071 (0.19)	0.2129 (0.32)	0.05029 (0.30)	195.0 (0.7	196.0 (1.2)	209 (14)
JLO05-6-27												
A, 2	23	187	7.6	435	26.1	0.33	0.04094 (0.17)	0.2913 (1.2)	0.05160 (1.1)	258.7 (0.9)	259.6 (5.4)	268 (50/52)
B, 3	12	314	10.5	129	71.3	0.31	0.03395 (0.44)	0.2341 (2.2)	0.05001 (1.9)	215.2 (1.9)	213.5 (8.3)	195 (88/93)
C, 4	12	260	8.1	362	17.7	0.28	0.03165 (0.17)	0.2252 (2.0)	0.05160 (1.9)	200.9 (0.7)	206.2 (7.5)	268 (86/91)
D, 4	11	200	7.3	392	13.3	0.34	0.03670 (0.18)	0.2626 (2.4)	0.05191 (2.3)	232.3 (0.8)	237 (10)	281 (101/108)
E, 1	6	333	9.4	975	3.8	0.19	0.02940 (0.14)	0.2031 (0.60)	0.05011 (0.57)	186.8 (2.1)	187.7 (2.1)	200 (26/Λ27)
F, 1	5	484	15.6	951	5.2	0.29	0.03276 (0.18)	0.2324 (0.54)	0.05145 (0.49)	207.8 (2.1)	212.2 (2.1)	261 (22/23)
G, 1	4	188	6.2	1056	1.5	0.26	0.03353 (0.19)	0.2340 (0.95)	0.05062 (0.89)	212.6 (3.6)	213.5 (3.6)	224 (41/42)

[1] All zircon grains selected for analysis were air abraded prior to dissolution. Fraction ID (capital letter - zircon A, B, etc.; titanite: T1, T2, etc.), followed by the number of grains

[2] U blank correction of 1pg ±20%; U fractionation corrections were measured for each run with a double ^{233}U-^{235}U spike.

[3] Radiogenic Pb

[4] Measured ratio corrected for spike and Pb fractionation of 0.32-0.37/amu ± 20% (Daly collector) which was determined by repeated analysis of NBS Pb 982 standard throughout the course of this study.

[5] Total common Pb in analysis based on blank isotopic composition.

[6] Model Th/U derived from radiogenic ^{208}Pb and the $^{207}Pb/^{206}Pb$ age of fraction

[7] Blank and common Pb corrected; Pb procedural blanks were ~1.5-5 pg and U <1 pg. Common Pb concentrations are based on Stacey-Kramers model Pb at the interpreted age of the rock or the $^{207}Pb/^{206}Pb$ age of the rock (Stacey and Kramers, 1975).

monitor. The best statistically justified plateau and plateau age were picked based on the following criteria:

- three or more contiguous steps comprising more than 30% of the ^{39}Ar;
- the probability of fit of the weighted mean age greater than 5%;
- the slope of the error-weighted line through the plateau ages equals zero at 5% confidence;
- the ages of the two outermost steps on a plateau are not significantly different from the weighted-mean plateau age (at 1.8σ, six or more steps only); and
- the outermost two steps on either side of a plateau must not have nonzero slopes with the same sign (at 1.8σ, nine or more steps only).

Analytical results for $^{40}Ar/^{39}Ar$ are presented in Table 3. A discussion of results in a geological context follow in these sections: 'Iron Mask', 'Mount Polley', 'Shiko Lake Stock', 'Woodjam Property' and 'Gavin Lake'.

IRON MASK BATHOLITH

The Iron Mask batholith is a northwest-trending, diorite-monzonite complex that intruded Carnian to Norian volcanic and sedimentary rocks of the eastern Nicola Group (Preto, 1979; Mortimer, 1987). It consists of two separate bodies: the 22 km long by 5 km wide Iron Mask batholith (Fig 2) in the southeast and the smaller, 5 km by 5 km Cherry Creek pluton in the northwest (Preto 1967, 1972; Northcote, 1974). The two are separated by an east-trending graben filled with Eocene Kamloops Group volcanic and sedimentary rocks. Snyder and Russell (1993, 1995) have described the various phases of the batholith and studied the petrogenetic relationships between them, as

well as an enigmatic picrite unit (Snyder and Russell, 1994). We follow their revised sequence of major intrusions (from oldest to youngest): Pothook diorite, Cherry Creek monzonite and Sugarloaf diorite. Many previous maps show a fourth phase, the Iron Mask Hybrid phase. Snyder and Russell assert that the Hybrid is mainly Pothook diorite containing abundant, variably assimilated Nicola Group xenoliths. Our observations confirm this assertion; however, xenolith-rich Sugarloaf diorite can also form a Hybrid look-alike unit (Logan and Mihalynuk, 2005a).

Chemically distinctive hydrothermal mineralization overprints each intrusive phase. Auriferous, fracture-controlled chalcopyrite and bornite with magnetite accompanies the potassic alteration associated with the Cherry Creek monzonite and the sodic alteration overprint on the Sugarloaf diorite. Alteration and mineralization tend to focus along intrusive contacts between the older Pothook/Hybrid phases and the younger feldspar and hornblende-phyric phases. To date, no significant mineralization has been delineated outside the batholith in the Nicola Group volcanic rocks (although Nicola Group strata are an important host of mineralization at Copper Mountain, 140 km to the south).

TABLE 2. LASER ABLATION INDUCTIVELY COUPLED PLASMA MASS SPECTROMETRY (ICP-MS) U-PB DATA.

Analysis	Isotopic Ratios ±1σ, absolute				ρ^1	Age ±1σ, Ma	
	$^{207}Pb/^{235}U$	1σ error	$^{206}Pb/^{238}U$	1σ error		$^{206}Pb/^{238}U$	1σ error
JL1	0.26530	0.00766	0.0363	0.00032	0.3053	229.9	2.0
JL2	0.19386	0.01171	0.0247	0.00049	0.3284	157.3	3.1
JL3	0.24811	0.00761	0.03389	0.00031	0.2982	214.8	1.9
JL4	0.25834	0.01256	0.03482	0.00049	0.2894	220.6	3.1
JL5	0.23832	0.03454	0.03449	0.00088	0.1760	218.6	5.5
JL6	0.16866	0.03324	0.02553	0.00100	0.1987	162.5	6.3
JL7	0.29456	0.01547	0.03711	0.00052	0.2668	234.9	3.3
JL8	0.19618	0.01262	0.02473	0.00054	0.3394	157.5	3.4
JL9	0.26353	0.01534	0.03697	0.00064	0.2974	234.0	4.0
JL10	0.16756	0.00858	0.02475	0.00042	0.3314	157.6	2.6
JL11	0.16777	0.05188	0.02446	0.00178	0.2353	155.8	11.2
JL12	0.17405	0.00604	0.02567	0.00028	0.3143	163.4	1.8
JL13	0.18526	0.01492	0.02448	0.00070	0.3551	155.9	4.4
JL14	0.17508	0.02564	0.02461	0.00105	0.2913	156.7	6.6

[1] Estimate of correlation coefficient (ρ) given by [% error $^{206}Pb/^{238}U$ /% error $^{207}Pb/^{235}U$].

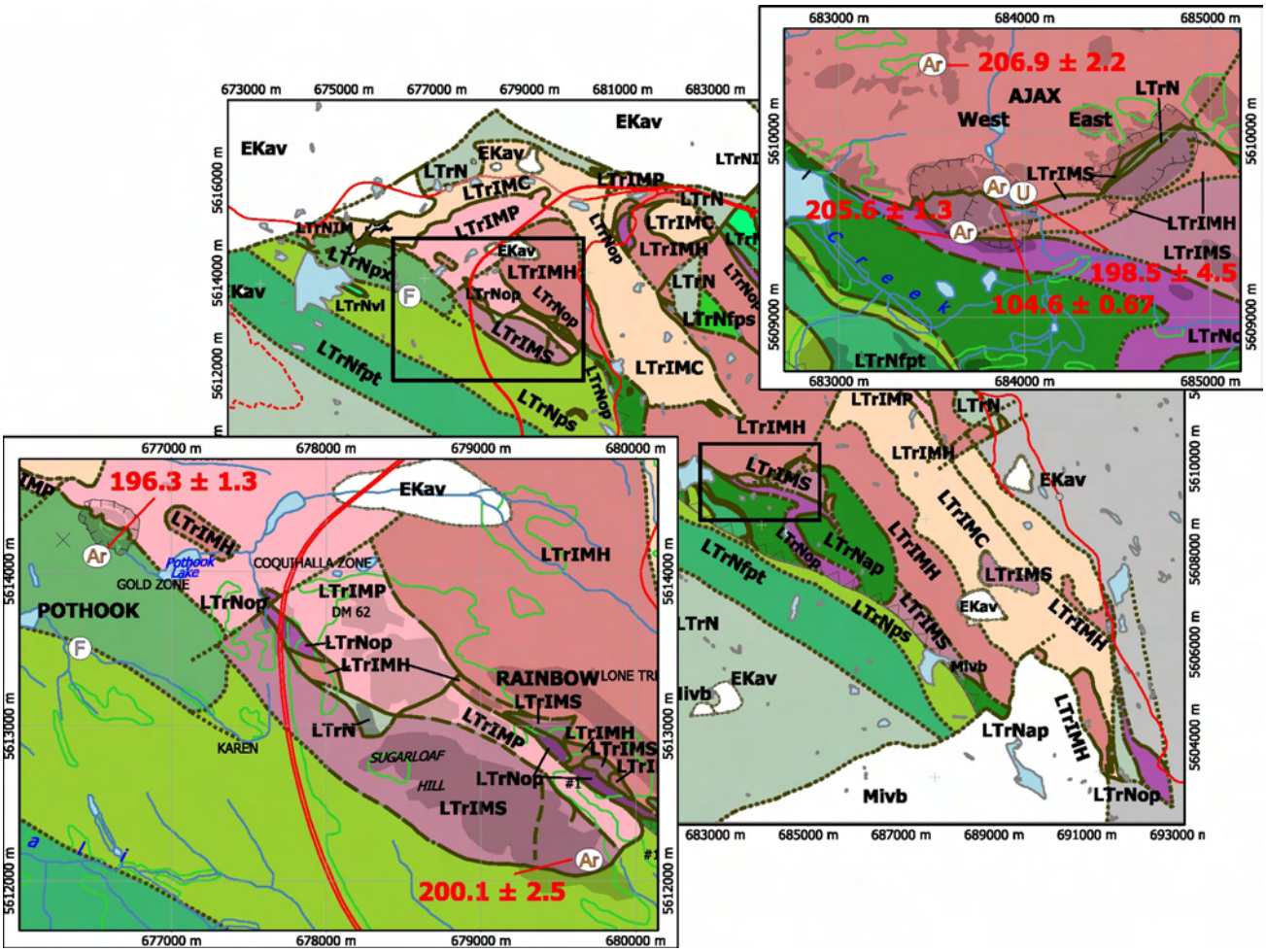

Figure 2. Compilation map of the Iron Mask batholith (*modified from* Logan *et al.*, 2006).

Potassium-argon biotite cooling ages for samples of the Hybrid and Cherry Creek phases and hydrothermal alteration associated with mineralization (Preto *et al.,* 1979) range from 201 to 209 Ma (mean 204 ±12 Ma). The U-Pb age data for samples of the Pothook, Hybrid and Cherry Creek phases of the batholith (Mortensen *et al.,* 1995) are 204 ±3 Ma. Sugarloaf diorite is the youngest phase of the Iron Mask batholith. According to Ross *et al*. (1995), it is responsible for albitic alteration and copper-gold mineralization. Attempts to extract zircon from this unit have hitherto been unsuccessful.

Samples of the Iron Mask were collected from five separate sites along the southwestern margin of the batholith (Fig 2). Sampling includes a pegmatitic variety of the Iron Mask Hybrid phase, foliated augite crystal tuff of the Nicola Group, two hornblende diorite samples of the Sugarloaf phase and hydrothermal titanite from a mineralized vein in the Ajax West pit. Sample descriptions and data interpretation are below.

Iron Mask Hybrid (MMI-04-4-1A)

The Iron Mask Hybrid phase is a xenolith-rich, heterogeneous unit that comprises approximately 45% of the Iron Mask batholith (Fig 2). Hybrid rocks mark the contact zones between individual phases (*i.e.,* Pothook, Cherry Creek and Sugarloaf) within the batholith, as well as the contact zones between the margin of the batholith and the volcanic country rock. A xenolith-poor intrusive breccia occupies a northerly trending belt, extending from the Ajax deposit to Coal Hill. Here, it is fine-grained to pegmatitic with local trachytic segregations of clinopyroxene, plagioclase, hornblende and magnetite. North of the Ajax deposit, the hybrid rocks possess a consistent east-trending magmatic foliation and pegmatitic mineral growth direction is perpendicular to the magmatic foliation, probably parallel to the direction of dilatancy (Fig 10; Logan and Mihalynuk, 2005b).

Coarse-grained hornblende crystals that define this well-developed mineral lineation were selected and dated with $^{40}Ar/^{39}Ar$ step-heating techniques to constrain the timing of crystal growth and cooling history (hornblende closure temperature of 550°C; Harrison, 1981). The hornblende separate (MMI-04-4-1A) yields a good 206.9 ±2.2 Ma age spectrum with a strong plateau representing 97.7% of the total ^{39}Ar released (Fig 3a). The inverse isochron plot gave an atmospheric intercept of 285 ±25 Ma and an isochron age of 207.1 ±1.3 Ma, which agrees within error to the calculated plateau age. Preto *et al*. (1979) reported a biotite K-Ar age for a sample of the Iron Mask Hybrid phase from a similar location with a cooling age of 204 ±12 Ma, equivalent within the limits of error.

Foliated Pyroxene-Porphyritic Basalt (JLO-04-17a)

On the south side of the Ajax west pit decline, foliated, carbonate-altered augite crystal tuff, augite porphyry basalt and picrite are intruded by a 1.2 m thick Sugarloaf dike. Both the foliation and the dike are warped by a gentle upright fold. The foliation and the fold axial plane average 120°/60° mineral elongation lineation developed around pyroxene porphyroblasts in the adjacent picrite trend 10°/115°.

The foliated augite tuff was collected and a sample of sericite that defines the fabric (Fig 4) was dated using $^{40}Ar/^{39}Ar$ step-heating techniques to constrain the timing of foliation generation. The age spectra are complicated and the four-point inverse isochron plot is unusable. The heating data indicates probable excess argon in the low-temperature steps (1–5) and high Ca/K ratios indicative of contamination in the high-temperature steps (11–16). The four-step plateau age of 205.6 ±1.3 Ma is defined by 37% of the total ^{39}Ar (Fig 3b). In spite of the high Ca/K ratios, the last 4 high-temperature steps yield a *ca*. 189 Ma age with 20% of the ^{39}Ar. An accurate assessment of the metamorphic age cannot be derived from these data, but a Late Triassic to Early Jurassic age for crystallization of the sericite is indicated.

Sugarloaf Hill Monzodiorite (JLO-04-6-67)

The Sugarloaf Hill stock is one of the lenticular northwest-trending intrusions of Sugarloaf monzodiorite that are dispersed primarily along the western margin of the batholith. These stocks are associated with Cu-Au porphyry mineralization at the past-producing Ajax East deposit and at the Rainbow deposit, which has drill-indicated resources from the #2 and #22 zones of 21.9 million tonnes grading 0.464% Cu and 0.106 g/t Au (0.30% Cu cut-off; Abacus Mining and Exploration Corporation, 2006). The Rainbow property is located on the eastern slopes of Sugarloaf Hill, close to the Leemac fault. The #1 and #17 zones are hosted in Sugarloaf hornblende porphyry; the #2 and #22 zones in Pothook/Sugarloaf hybrid and metavolcanic rock, respectively (Logan and Mihalynuk, 2005b). All mineralization is fracture or breccia-controlled and consists of chalcopyrite±magnetite accompanied with pyrite and alteration mineralogy.

According to Oliver (1995), Sugarloaf Hill is underlain by three mappable stocks: hornblende diorite, albite-phyric monzodiorite and a microphyric hornblende diorite. Snyder and Russell (1993) interpreted the radial distribution of hornblende porphyry dikes around Sugarloaf Hill as evidence that the stock was a subvolcanic intrusive centre. The stocks intrude picrite and volcaniclastic units of the Nicola Group. On their northeast margin, the Sugarloaf Hill stocks are faulted and structurally interleaved along the Leemac fault with the Hybrid and Pothook phases.

A sample of least altered, medium-grained hornblende-porphyritic monzodiorite was collected from the southeastern end of the stock (Fig 2) for chemical and age determination. The diorite is characterized by 1 to 3 mm euhedral hornblende (20%) and plagioclase (35%) phenocrysts in a fine-grained groundmass of plagioclase, clinopyroxene, magnetite and potassium feldspar. Accessory minerals include apatite, sphene, magnetite, pyrite and traces of quartz. Minor alteration products include actinolite, sericite and calcite.

A hornblende separate was dated by $^{40}Ar/^{39}Ar$ step-heating techniques to constrain the cooling age of the intrusion. Analyses of hornblende from JLO-04-6-67 gave a good age spectrum, showing some Ar loss in the early heating stages and a cooling age of 200.1 ±2.5 Ma using 6 of 11 steps and 89.2% of the ^{39}Ar (Fig 3c). The inverse isochron plot gave an atmospheric intercept of 263 ±84 Ma and an isochron age of 202.2 ±6.1 Ma, which agrees within error to the calculated plateau age.

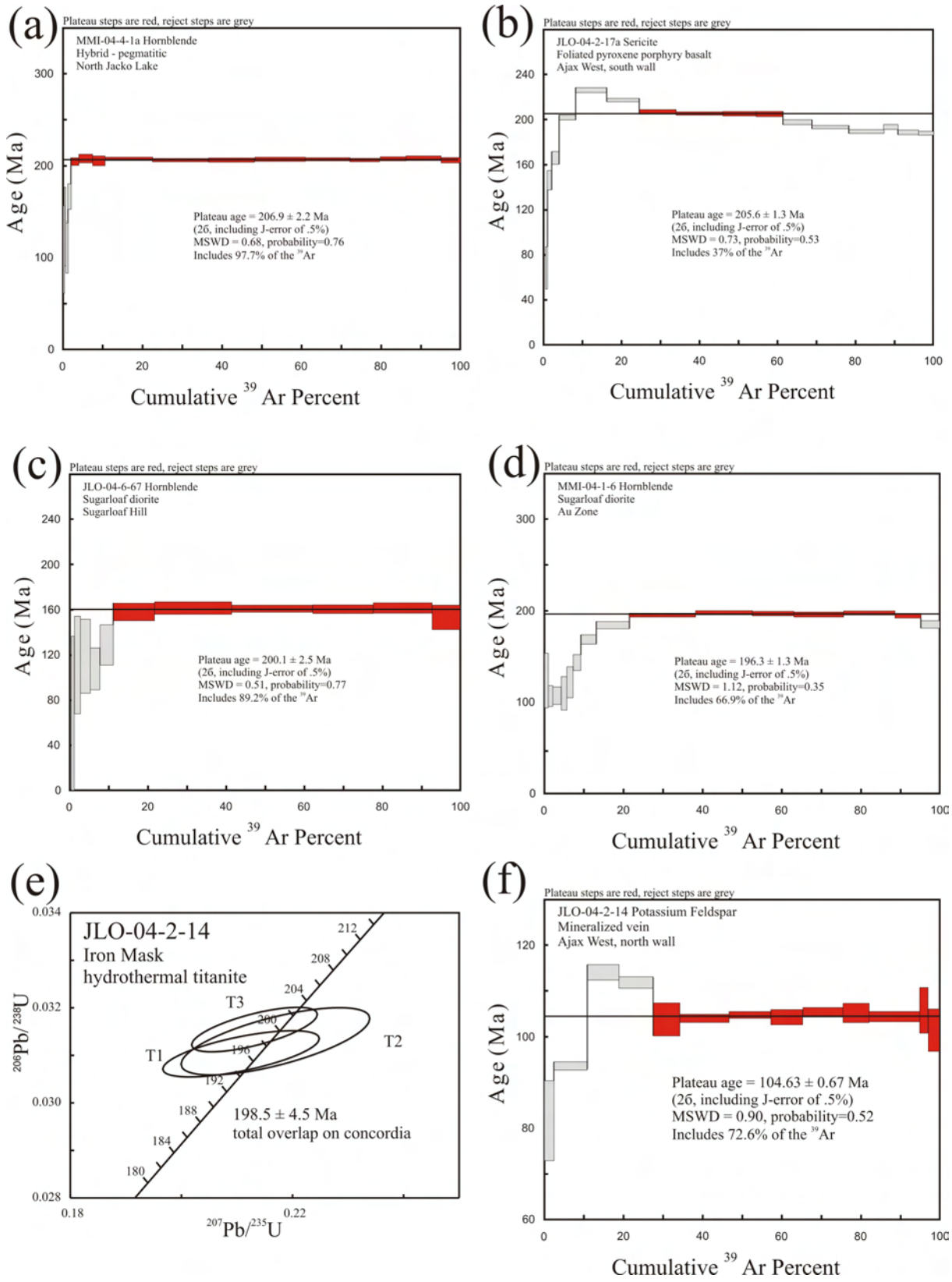

Figure 3. Step-heating gas release plots for $^{40}Ar/^{39}Ar$ analyses for a) hornblende sample MMI-04-4-1a from North Jacko Lake; b) sericite sample JL0-04-2-17a from Ajax West, south wall; c) hornblende sample JLO-04-6-67 from Sugarloaf Hill; d) concordia plot of U-Pb thermal ion mass spectrometry (TIMS) data for samples from the Iron Mask batholith; e) step-heating gas release plots for $^{40}Ar/^{39}Ar$ analysis for potassium feldspar sample JLO-04-2-14 from Ajax West, north wall; T1, T2 and T3 *e* correspond to fraction numbers in Table 1. All errors are displayed as 2σ level of uncertainty.

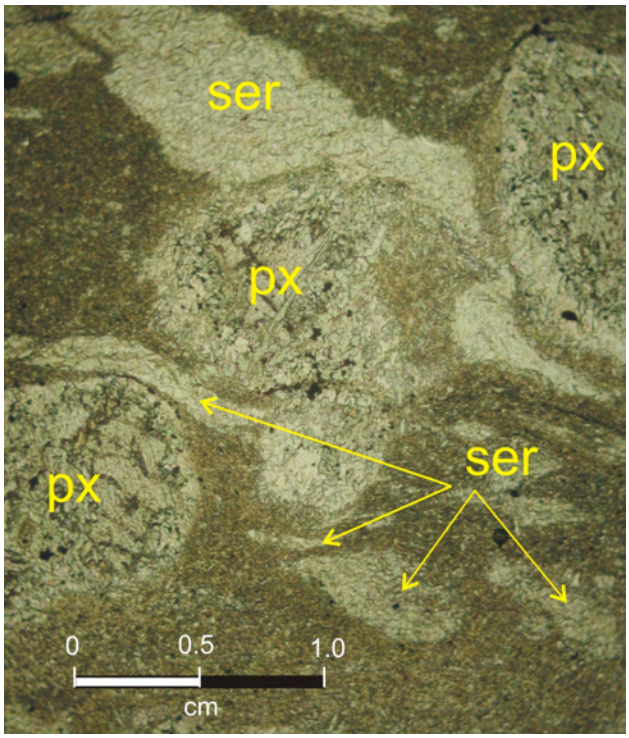

Figure 4. Photomicrograph of foliated and weakly crenulated sericite porphyroblastic augite crystal tuff (JLO-04-17a); plane-polarized light. Abbreviations: px, pyroxene; ser, sericite.

Gold Zone, Sugarloaf Dike (MMI-04-1-6)

Gold-rich, copper-poor mineralization occurs in two northwest-trending zones (Gold and East) that are located immediately southwest of the Pothook pit (Fig 2). The Gold zone was first recognized by Teck Cominco in the 1990s at the structurally complicated contact between the Pothook and Cherry Creek phases and the Nicola Group country rocks. Another feature of the Gold zone is a northwesterly swarm of Sugarloaf diorite dikes at the southern margin of the broad propylitic alteration zone, which extends to the northern Afton pit, where it is an important part of the mineralizing system.

Sugarloaf dikes in the Gold zone are weakly trachytic, hornblende-porphyritic diorite with a moderate to strong albitic and propylitic overprint. An ICP-MS analysis of one of the dikes that returned 480 ppb Au and 161 ppm Cu. Reported drill intersections of >0.2% Cu and >0.2 g/t Au characterize the mineralized zone, with higher-grade intersections up to 3.0 g/t Au (Evans, 1992). Grab samples from the southeast end of the East zone returned gold-rich assays of 6.36 g/t Au, 0.83 g/t Pd and 1.0% Cu (Abacus News Release, Dec 17, 2002).

A sample of one of the least-altered Sugarloaf dikes was collected from the Gold zone to establish the crystallization age and to provide constraints on the cooling history for the hydrothermal mineralizing system responsible for the gold-rich, copper-poor mineralization. Although the age spectrum shows Ar loss in the early heating steps and a slightly hump-shaped pattern, a good plateau is defined by five steps representing more than 66% of the total ^{39}Ar released (Fig 3d). The 196.3 ±1.3 Ma hornblende cooling age is interpreted to represent the magmatic crystallization age.

Hydrothermal Titanite and Potassium Feldspar (JLO-04-2-14)

The Ajax West and Ajax East deposits are located on the southwest side of the Iron Mask batholith at the contact between medium to coarse-grained Iron Mask Hybrid diorite and Sugarloaf diorite (Fig 2). Mineralization occurs as disseminated and veinlet chalcopyrite in propylitic, albitic and potassic-altered Sugarloaf diorite. In the west deposit, a core of intense albite alteration diminishes outward to less pervasive peripheral propylitic alteration (chlorite, epidote, calcite±pyrite; Ross *et al.,* 1995). Outside the ore shell, but within the propylitic alteration zone in the north wall of the West pit, *en échelon* northwest-striking (300°/62°) salmon-pink potassium feldspar veins (10–50 cm) cut Iron Mask Hybrid rocks. These veins have a margin of magnetite intergrown with biotite±chlorite and a core of a vuggy intergrown aphyric matrix of potassium feldspar and albite with calcite, chalcopyrite, pyrite and coarse euhedral crystals of titanite-filling fractures and interconnected vugs (Fig 18; Logan and Mihalynuk, 2005b).

Titanite was separated from the hydrothermal vein assemblage and analyzed using U-Pb TIMS geochronological techniques to provide a maximum age limit on the chalcopyrite mineralization hosted within the vein set. One large (~0.5 cm), pale yellow, clear to slightly cloudy, striated titanite grain was removed from a vug and broken into fragments. Three of the clearest of these were analyzed and gave concordant and overlapping results. A crystallization age of 198.5 ±4.5 Ma is based on the total range of ^{206}Pb/^{238}U ages and associated 2σ errors for the three results (Fig 3e, Table 1).

In addition to titanite, potassium feldspar was separated from the vein assemblage and dated with ^{40}Ar/^{39}Ar step-heating techniques to constrain the cooling history of the hydrothermal vein mineralization. The potassium feldspar has a complex age spectra with older apparent ages in the low-temperature steps (Fig 3f). A plateau age of 104.63 ±0.67 Ma calculated from the final 72.6% of the ^{39}Ar provides a good cooling age, which is interpreted as the hydrothermal crystallization age of the feldspar. An inverse isochron plot gave an isochron age of 103.6 ±2.9 Ma, which agrees within error to the calculated plateau age.

CENTRAL QUESNEL BELT

The Nicola Group of the central Quesnel belt consists of a two-fold subdivision: a lower fine-grained Middle to Upper Triassic sedimentary succession and an upper 'alkalic or shoshonitic' sequence of Upper Triassic calcalkaline arc volcanic deposits, which are gradational with and conformably overlie the sedimentary package. Lower to Middle Jurassic sedimentary and less common volcanic rocks unconformably overlie the Nicola Group (Logan and Mihalynuk, 2005a, b). A number of small composite granitic bodies intrude the area. Data from this study and others (Breitsprecher and Mortensen, 2004) indicate the presence of at least five intrusive suites: Late Triassic (Granite Mountain suite, *ca*. 212 Ma), latest Late Triassic (Mount Polley intrusive suite, *ca*. 205 Ma), Early Jurassic (Takomkane-Thuya suite, *ca*. 193 Ma), Middle Jurassic (Gavin Lake suite, *ca*. 163 Ma) and mid-Cretaceous (Naver suite, *ca*. 106 Ma).

An axis of alkalic intrusions and related mineralization occupies the eastern part of the Quesnel Arc in central British Columbia (Fig 8 *in* Panteleyev *et al.,* 1996). Fewer and more widely spaced mineral occurrences associated with calcalkaline intrusions are located on the western margin of Quesnellia.

In the area surrounding Mount Polley, there are a number of small, high-level composite intrusions composed of diorite through monzonite to syenite compositions. These are interpreted to have been emplaced into the upper levels of the arc and are often hosted by coarse, extrusive-facies volcanic rocks that indicate individual eruptive centres (*i.e.*, Mount Polley, Bailey and Hodgson, 1979; Shiko Lake, Panteleyev *et al.,* 1996). An extensive program of geological mapping and geochronology was conducted over the eastern Intermontane Belt in the Quesnel and Quesnel River areas by Bailey (1988, 1990), Panteleyev (1987, 1988) and Panteleyev *et al.* (1996). Geochronological samples were collected from the Mount Polley area as part of a regional mapping program in the Quesnel Lake (Fig 5) and Horsefly Lake (Fig 10) map areas in 2004 and 2005. Samples from the immediate vicinity of the Mount Polley mine include two from pyroxene monzonite satellite stocks, a potassium feldspar megacrystic dike, a quartz-phyric andesite and hydrothermal biotite from the Cariboo pit and the Northeast zone. Additional sampling was carried out at Shiko Lake (quartz syenite), Woodjam property (hornblende-quartz monzonite and quartz-feldspar porphyry) and Gavin Lake (quartz-porphyritic monzogranite). Sample descriptions and data interpretation are below.

MOUNT POLLEY INTRUSIVE COMPLEX (MPIC)

The Mount Polley alkalic intrusive complex is a north to northwest elongated, composite centre located in a large (40 by 17 km) regional aeromagnetic anomaly. This high-level intrusive complex is 5.5 by 4 km in size and comprised primarily of fine-grained porphyritic monzodiorite and monzonite, plagioclase porphyry and syenite stocks and dikes with abundant screens of metavolcanic rock and hydrothermal breccia (Fraser, 1994, 1995; Hodgson *et al.,* 1976), features characteristic of a subvolcanic environment (Fig 5). It is separated from another northwest-elongated composite intrusive body to the southwest across a ~1 km thick panel of volcanic strata. Known as the Bootjack stock, this second body is 2.3 by 7 km, is characterized by an unusual orbicular pseudoleucite syenite (Bath and Logan, 2006) and lacks subvolcanic textures.

Published geochronology from the Bootjack stock includes a hornblende $^{40}Ar/^{39}Ar$ plateau age of 203.1 ±2.0 Ma from the coarse-grained syenite phase (Bailey and Archibald, 1990), a U-Pb zircon age from the orbicular syenite (202.7 ±7.1 Ma; Mortensen *et al.,* 1995) and a Pb-Pb titanite age from pseudoleucite syenite (200.7 ±2.8 Ma; Mortensen *et al.,* 1995). Uranium-lead ages from two intrusive phases from the MPIC (201.7 ±4 Ma zircon from diorite and 204.7 ±3 Ma zircon from plagioclase porphyry) are similar, within error, to ages from the Bootjack stock (Mortensen *et al.,* 1995). Fraser (1995), however, infers that the Bootjack stock is younger than the MPIC on the basis of diorite xenoliths present within the nepheline pseudoleucite and orbicular syenite units. Such an age relationship can be accommodated by the error envelopes on the geochronological data from the MPIC and Bootjack stock.

Satellite Monzonite Stock (JLO-04-24-111)

A northwest-trending hypabyssal stock (1 km by 3 km) of pyroxene monzonite crops out northwest of Bootjack Lake. It consists of holocrystalline plagioclase-pyroxene-phyric monzodiorite and pink pyroxene monzonite. Rounded xenoliths of pyroxene porphyry and diorite are common. The stock is fine-grained, equigranular or microporphyritic and weakly trachytic. Petrographic observations reveal that both phases have the same modal mineralogy: sericitized plagioclase laths (45%, 1 mm), potassium feldspar (40%, <1 mm laths and matrix material) and euhedral pyroxene crystals (10–15%, 0.5–1 mm). Accessory minerals include magnetite, apatite and zircon. Potassium alteration is pervasive, flooding the matrix and as overgrowths on feldspar phenocrysts. Late-stage deuteric alteration has produced isolated patches of chlorite and calcite.

In places, the weathered surfaces of fine-grained monzonite display a crackle or autobrecciated texture. At its southern margin, the breccia is pink with clasts defined by a tight, anastomosing network of chlorite fractures. Nearer its centre, the stock is dominated by a potassic albite-altered breccia resembling the hydrothermal breccia at the Springer zone and on Mount Polley (Logan and Mihalynuk, 2005a).

A 20 kg sample was collected from a borrow pit located in the centre of the stock. This sample yielded clear, colourless, euhedral stubby zircon prisms and more commonly broken pieces. Five air-abraded multigrain fractions ranging from 3 to ~30 complete or broken grains were analyzed using the TIMS technique. Results indicate minor inheritance. An age estimate of 203.1 +1.6/–12.7 Ma (mean standard weighted deviate = 0.42) is based on the lower intercept of a five-point regression (Fig 6a). Due to very limited data dispersion near the low end of the regression line, the precision of the upper intercept is a very poor 1284 +1300/–872 Ma. This value gives an estimate for the average age of inheritance in analyzed grains.

Polley Lake Road, Monzonite (JLO-04-20-70b)

A small (<1 km^2), hypabyssal monzonite stock crops out north of the Polley Lake Road approximately 500 m east of the Frypan Road junction (Fig 5). The rock is a microporphyritic plagioclase-pyroxene-phyric monzonite, similar to the stock located northwest of Bootjack Lake (JLO-04-24-111). It is composed of roughly equal amounts of plagioclase (3–5 mm tabular laths), potassium feldspar (subhedral 2–3 mm grains and matrix material), 10 to 15% tabular euhedral pyroxene (0.7–1.5 mm) and trace hornblende and biotite. Accessory minerals include magnetite, sphene and apatite. Potassium alteration has created a turbid matrix and has replaced most of the feldspar phenocrysts. Late deuteric alteration caused chloritization of hornblende and biotite, but had little effect on pyroxene.

The stock intrudes altered breccia and clastic rocks of the Mount Polley intrusive complex very close to the erosional top of the Triassic section. Early Jurassic bedded volcaniclastic rocks, tuff (MMI-04-26-18) and conglomerate unconformably overlie the MPIC at this locality and al-

though the contact is not exposed on surface, it has been intersected in drilling (L. Ferreira, pers comm, 2005).

A hornblende separate from the monzonite was analyzed to estimate the age of the stock and the cooling history of the intrusive centre. The hornblende separate yielded a complicated hump-shaped age spectra, which is interpreted to indicate excess argon and possible ^{39}Ar recoil in the hornblende or the contained pyroxene inclusions (Fig 6b). If recoil is assumed, the integrated age (160.7 ±2.05 Ma) is usually the best age estimate; however, we tentatively accept the plateau age of 165.2 ±1.8 Ma (50.9% of the total ^{39}Ar released) as a better age approximation. We ascribe the complicated spectrum to the release of excess argon from chloritized hornblende during low-temperature heating steps and contamination (high Ca/K mineral, *i.e.,* pyroxene inclusions) during high-temperature steps.

Bell Pit, Potassium-Feldspar–Porphyritic Syenite (JLO-04-50-510)

Potassium-feldspar–porphyritic syenite occurs as dikes within the core of the stock underlying the top of Mount Polley peak (Central zone; Fraser, 1994) and as fragments in mineralized breccia at the Northeast zone and Lloyd-Nordic zone (Logan and Mihalynuk, 2005a). It is characterized by the presence of salmon-pink-coloured tabular orthoclase phenocrysts. An inverse relationship between the proportion of feldspar phenocrysts and their size results in crowded trachytic varieties that contain 20 to 25% phenocrysts that average less than 7 mm in size and those monzosyenite that contain fewer phenocrysts (2–10%) that can be greater than 2 cm in length. The groundmass consists of weakly aligned plagioclase crystals with interstitial clinopyroxene, biotite and lesser magnetite, sphene and apatite. Late deuteric alteration has sericitized the feldspar and replaced mafic minerals with a mixture of chlorite, white mica and carbonate.

Early exploration drilling of the Northeast zone led to the recognition of a close association between ore-grade mineralization and the appearance of potassium feldspar megacrystic syenite clasts in the breccia (P. McAndless, pers comm, 2005). Chilled margins and crosscutting relationships indicate the late intrusion of potassium feldspar porphyritic syenite dikes. In the intrusive sequence at Mount Polley, the porphyritic syenite was considered to be a good candidate for the 'causative' intrusion. To test this hypothesis, a 25 kg sample of potassium-feldspar–porphyritic syenite was collected from an east-southeast-trending dike that intrudes diorite in the highwall between the Bell and Cariboo pits. It was dated using U-Pb in zircons to determine a magmatic crystallization age.

Zircons recovered are both euhedral, rounded and slightly resorbed clear prisms and grain fragments. Three abraded multigrain fractions give concordant and overlapping results (Fig 6c) that yield a concordia age of 205.01 ±0.3 Ma (mean standard weighted deviate = 3.3; probabil-

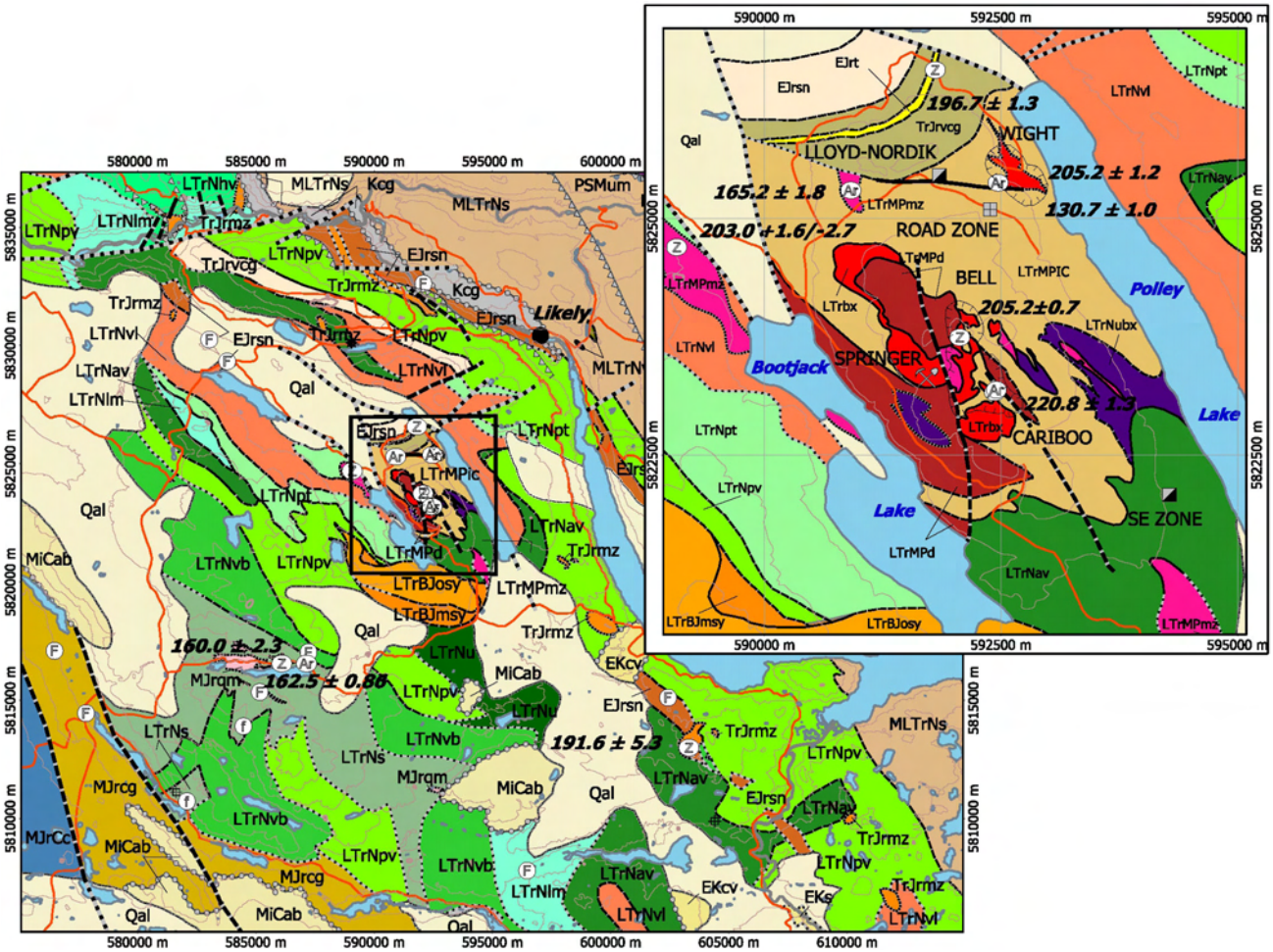

ity of concordance = 0.071; Ludwig, 2003). We consider this to be the crystallization age for the potassium-feldspar–porphyritic dike.

Cariboo Pit, Hydrothermal Biotite (MMI-04-24-1)

Mineralization at Mount Polley is hosted by a variety of hydrothermal breccia that cut a high-level multiphase dioritic-monzonitic intrusive sequence. Alteration and mineralization are interpreted to be related to a single hydrothermal centre (Hodgson *et al.,* 1976; Bailey and Hodgson, 1979) modified by faulting (Fraser, 1994). The breccia and hydrothermal alteration, however, imposed on them display sufficient zonal variation to warrant subdivision into the West (Springer), Central (Cariboo and Bell), Northeast and Southeast zones (Fig 16; Logan and Mihalynuk, 2005a).

Work by Fraser (1994, 1995) in the Central and West zones resulted in the subdivision of the potassic core into three subzones defined on the basis of the dominant alteration mineral: biotite, actinolite or potassium feldspar albite. The biotite and actinolite subzones overprint the Central zone east of the Mount Polley fault; the potassium feldspar albite zone occurs west of the fault in a northwest-trending belt west of Mount Polley (West zone). Farther west still is the actinolite zone.

A sample of coarse hydrothermal biotite was collected from the east wall of the Cariboo pit in the biotite subzone of the potassic core zone (Fraser, 1995). This zone is characterized by coarse, secondary biotite developed within the matrix of mineralized hydrothermal breccia in the core of the Central zone.

The biotite separate yielded a normal diffusive loss profile in the low-temperature steps. Apparent ages increase over the initial 45% of the ^{39}Ar released. The remainder of the spectra is fairly constant and gave a weighted mean age of 220.8 ±1.3 Ma (Fig 6d). The inverse isochron plot gave an atmospheric intercept of 280 ±31 Ma and an isochron age of 221.4 ±1.6 Ma, which agrees, within error to the calculated plateau age. The biotite plateau age for sample MMI-04-24-1 predates the intrusion of the alkaline MPIC rocks by approximately 15 Ma, and is herein considered suspect.

Northeast Zone, Hydrothermal Biotite and Orthoclase (WB-05-209)

The Northeast zone is a 150 by 500 m northwest-trending, steeply dipping tabular zone of Cu-Au-Ag miner-

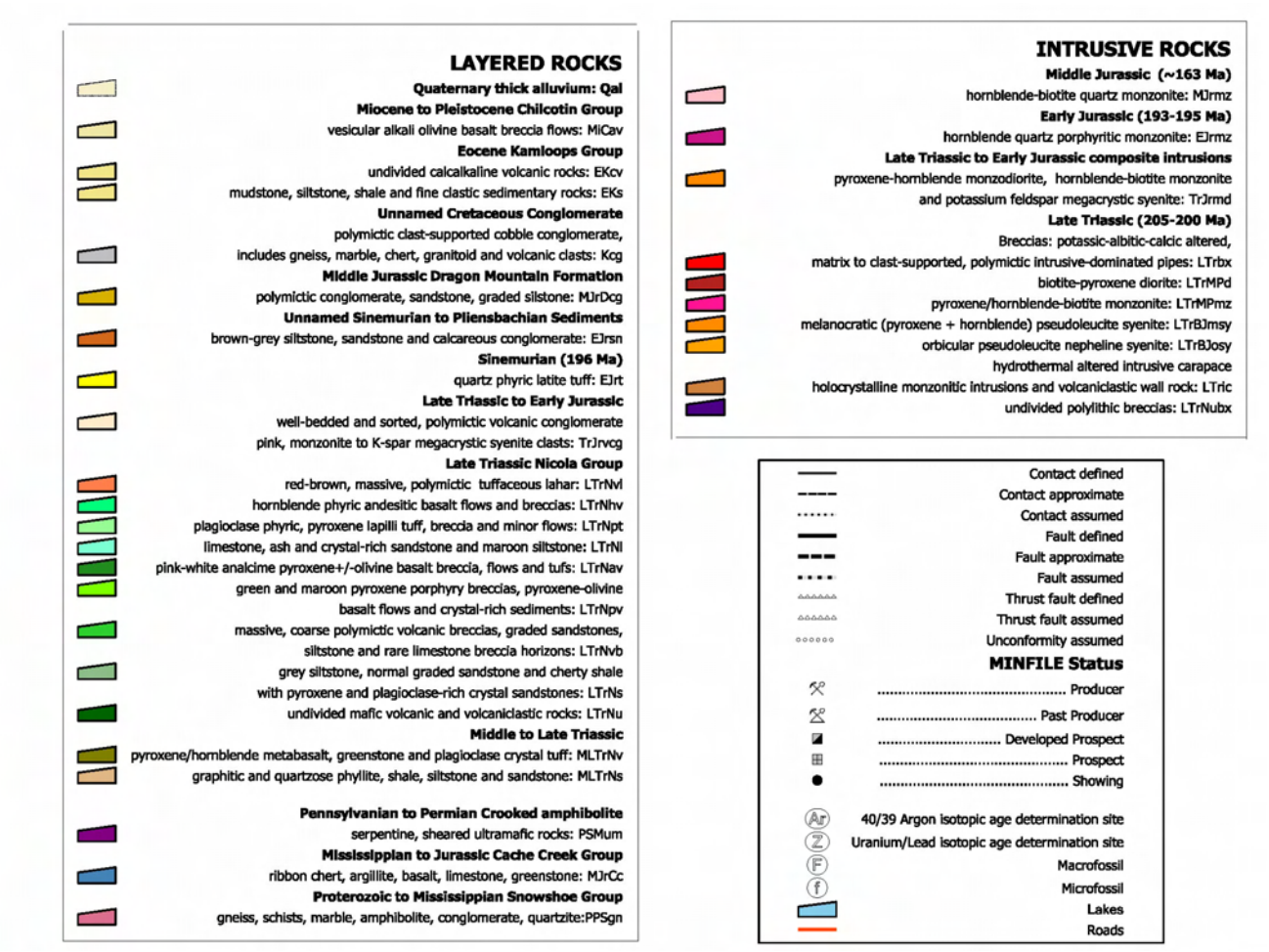

Figure 5. Regional geology map of the Mount Polley area with the location of geochronological samples. Inset shows the detailed area of the Mount Polley intrusive complex (MPIC); *modified from* Logan *et al.* (2007).

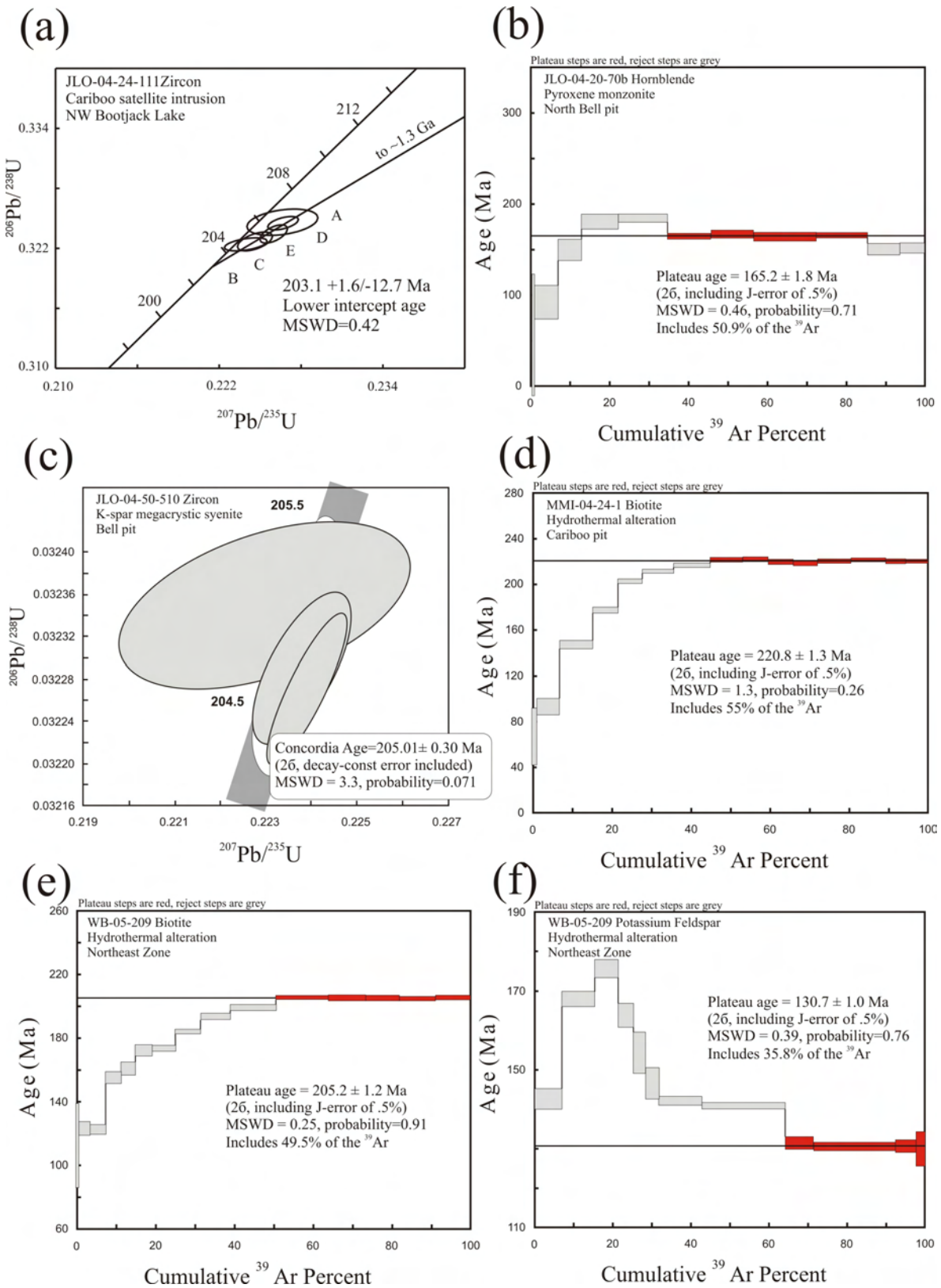

Figure 6. a) Concordia plot of U-Pb thermal ion mass spectrometry (TIMS) data for zircon samples JLO-04-24-111 from northwest Bootjack Lake; A, B, C, D and E correspond to fraction numbers in Table 1; b) step-heating gas release plot for $^{40}Ar/^{39}Ar$ analyses for hornblende samples JLO-04-20-70b from the North Bell pit; c) concordia plot of U-Pb TIMS data for zircon samples JLO-04-50-510 from the Bell pit; d) step-heating gas release plot for $^{40}Ar/^{39}Ar$ analyses for biotite samples MMI-04-24-1 from the Cariboo pit; e) step-heating gas release plot for $^{40}Ar/^{39}Ar$ analyses for biotite samples WB-05-209 from the Northeast zone; f) step-heating gas release plot for $^{40}Ar/^{39}Ar$ analyses for potassium feldspar samples WB-05-209 from the Northeast zone.

alized breccia located close to the northern margin of the MPIC. Alteration at the Northeast zone is similar to that present at the Central and West zone (1.5 km southwest). There are, however, subtle differences, plus mineralization is higher-grade overall with higher Cu:Au ratios, higher silver and bornite content, lower magnetite and higher copper grades, which make it an important exploration target.

A comprehensive petrographic study, augmented by SEM work on the mineralogy at the Northeast zone was completed by Ross (2004) in an unpublished report for Imperial Metals (summarized *in* Logan and Mihalynuk, 2005a). Ongoing research on the Northeast zone includes melt inclusion studies by A. Bath, carbonate geochemistry by H. Pass (both at CODES, University of Tasmania) and breccia genesis and alteration mineralogy by M. Jackson (MDRU, University of British Columbia).

Biotite is not a common alteration mineral in the Northeast zone, but a mineralized sample containing biotite was sampled from a 7 cm section of split drillcore from 289 m below the collar of diamond drill hole WB-05-209 (kindly contributed by L. Ferreira, Imperial Metals Corporation). The section sampled consists of pervasive potassium-flooded, salmon-pink microporphyritic plagioclase monzonite breccia. The rock is crackle brecciated and variably replaced and veined by chalcopyrite and coarse biotite (1.5–2 mm books). Chalcopyrite and biotite are intimately intergrown and believed to be coeval (Fig 7). Both biotite and potassium feldspar were separated from this sample and analyzed to constrain the cooling history of the alteration and mineralizing system in the Northeast zone (Fig 6e, f).

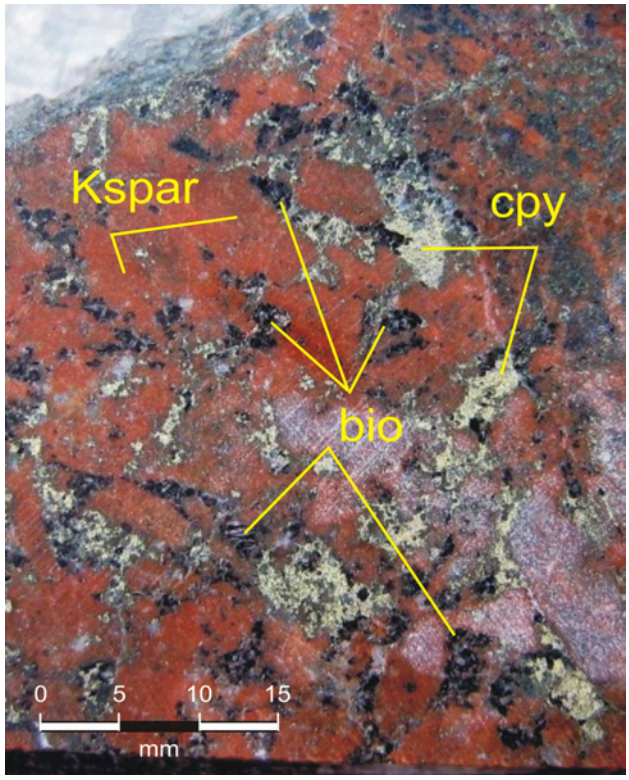

Figure 7. Diamond drill core sample (WB-05-209 at 289 m) of potassic-altered Northeast zone monzonite, showing coarse intergrowths of chalcopyrite and large books of secondary biotite sampled for $^{40}Ar/^{39}Ar$ age determination; abbreviations: cpy, chalcopyrite; kspar, potassium feldspar.

The increasing apparent ages displayed in the initial 50.5% of the biotite age spectrum represents a normal diffusion loss profile. A plateau age of 205.2 ±1.2 Ma calculated from the final 49.5% of the ^{39}Ar provides a good cooling age, which is interpreted as the crystallization age of the biotite. Potassium feldspar separated from the same sample has a complex age spectrum. A plateau age, using 35.8% of the ^{39}Ar in the last 5 heating steps, yielded 130.7 ±1.0 Ma. The potassium feldspar plateau age yields the same age, as do the lowest temperature steps of the biotite spectrum.

Quartz-Phyric Mauve Andesite (MMI-04-26-18)

Dense, quartz-phyric, white to mauve-weathering lapilli tuff is exposed in two outcrops between Bootjack and northern Polley lakes (Fig 3; Logan and Mihalynuk, 2005a). We used the field term 'mauve dacite' for this unit, but the SiO_2 content (<60%) indicates it is an andesite. It is crystal-rich, composed of tabular and broken plagioclase laths (40%, <3 mm), hornblende (3% altered 2–3 mm prisms), light grey quartz eyes (up to 1% and 5 mm diameter) and biotite (<1%, altered 2–3 mm booklets). The andesite contains undigested accidental fragments, shard-like crystal fragments, broken vesicular clasts and a devitrified glassy matrix (Fig 8). A vague compaction fabric is preserved locally, but clear evidence of collapsed pumice fragments or welding is absent. Possible collapsed pumice blocks are displayed in one outcrop below the Polley Lake road. For these reasons, we maintain that an extrusive origin (*i.e.,* ash flow) best accounts for the formation of this unit.

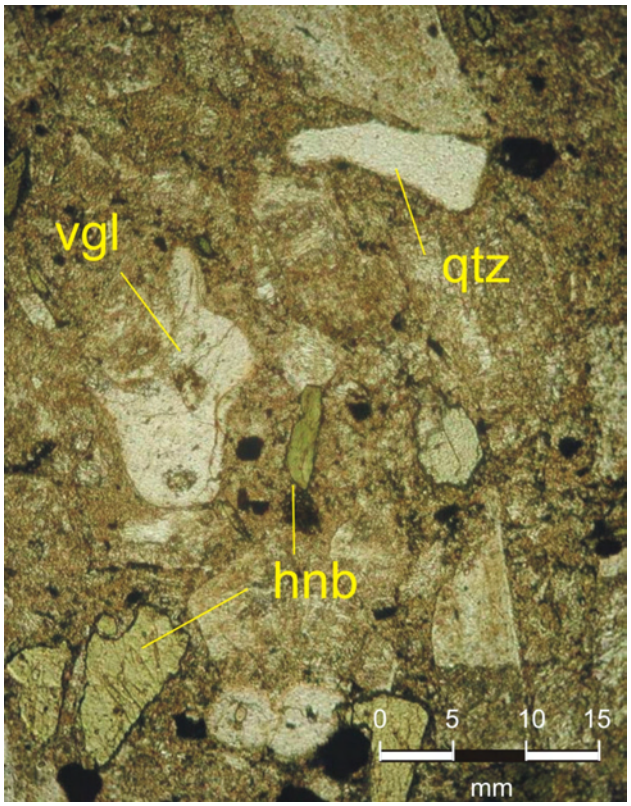

Figure 8. Quartz-phyric mauve andesite tuff. Note the devitrified glassy matrix, curviplanar fragments of vesicular glass (vgl) and crystal shards of hornblende (hnb) and quartz (qtz).

Bedding orientations of enclosing strata are parallel with the trend of the mauve andesite unit. A poorly exposed, probable gradational southern contact with the maroon laharic conglomerate is consistent with a pyroclastic origin and not a hypabyssal intrusion. This volcanic and epiclastic succession is unmineralized; it apparently overlaps mineralized breccia of the MPIC, thereby constraining the maximum age of mineralization.

Approximately 25 kg of the mauve andesite was collected for U-Pb analyses and a determination of a magmatic crystallization age to provide an age limit on the host volcanic stratigraphy. Abundant zircons were recovered from the sample. Zircons are vivid pink, stubby prismatic grains with abundant clear inclusions. Approximately 25 of the coarsest crystals were air abraded and run as 4 multigrain fractions of 2–6 grains each. The interpreted age of 196.7 ±1.3 Ma is based on two concordant ellipses on concordia (Fig 9a, d). Slightly younger U/Pb results for fractions B and E are attributed to minor Pb loss (Fig 9a).

SHIKO LAKE STOCK

A high-level alkalic stock intrudes Early Jurassic arc strata 15 km southeast of Mount Polley mine, near Shiko Lake (Fig 5). Three separate intrusive phases comprise the stock. These are, from oldest to youngest: a melanocratic, medium-grained, equigranular, biotite-pyroxene monzodiorite; a pink trachytic, medium to coarse-grained, potassium-feldspar–phyric syenite and a leucocratic alkali feldspar quartz syenite. The quartz syenite truncates a well-developed west-striking, 30° north-dipping trachytic fabric in the potassium feldspar megacrystic syenite, which veins and engulfs the earlier diorite. All phases contain mafic xenoliths of olivine-pyroxene-phyric basalt, fine-grained metasedimentary rocks and subvolcanic diorite to monzonite. Xenoliths increase in abundance toward the contact of the stock (Logan and Mihalynuk, 2005a).

Chalcopyrite and minor bornite occur as veins and disseminated clots within all three intrusive phases. Veins cutting the stock are intergrowths of actinolite, potassium feldspar, sphene, magnetite, and pyrite±chalcopyrite. Potassic overgrowths on feldspars and the replacement of hornblende by actinolite and biotite by chlorite are attributed to late deuteric alteration.

Potassium-argon biotite cooling dates on samples from the monzonitic core are reported by Panteleyev *et al.* (1996) as 192 ±10 Ma and 182 ±6 Ma, and from a hornblende porphyry dike cutting the stock as 196 ±7 Ma. A number of macrofossil identifications from the sedimentary rocks intruded by the Shiko stock are Early Jurassic (GSC-C-118687, probable Sinemurian; GSC-C-118685, Lower Sinemurian or possibly Hettangian; GSC-C-118686, Lower Sinemurian, lower Pliensbachian; Tipper, *in* Panteleyev *et al.,* 1996). Panteleyev *et al.* (1996) describe volcanic and intrusive breccia along the southern contact of the stock, which they interpreted to represent the vent zone of an intrusive centre.

Leucocratic Quartz Syenite (JLO-04-21-84)

The leucocratic quartz syenite is a medium to fine-grained equigranular rock characterized by quartz-filled miarolitic cavities and a negligible magnetic susceptibility. It is composed of interlocking tabular plagioclase laths (30%, <1 mm), equant orthoclase crystals (50%, 1–1.5 mm), interstitial vitreous quartz (18%), rare chloritic hornblende (3%, <1 mm) and biotite (<1%, altered <1 mm booklets). Accessory minerals include zircon, present as crystal aggregates or small euhedral crystals, apatite, calcite and pyrite.

A 20 kg sample of leucocratic quartz syenite was collected from a quarry at the western end of the stock for an age determination. It was selected because it is demonstratively the youngest mineralized phase. In addition, it is quartz saturated and possibly unrelated to other mineralized alkaline bodies in the Quesnel belt. The sample yielded clear, amber, euhedral to subhedral broken zircon crystals and a smaller population of complete grains of zircon. Approximately 30 of the best-quality grains (pieces and available complete crystals) were selected for analysis (*see* photo) and were strongly air abraded. During this process, much of the material was broken along internal fractures, ending up as smaller subrounded pieces. The clearest of these fragments (n = 6–10 per fraction) were selected for analysis. Uranium-lead results for the five analyzed fractions reflect minor Pb loss only; results are 0 to 3.5% discordant. The age estimate of 191.6 ±5.3 Ma is based on the calculated $^{207}Pb/^{206}Pb$ weighted mean, which is equivalent to the upper intercept of a regression anchored through 0 m.y. and all five fractions, as shown on standard concordia plot for this sample (Fig 9b).

WOODJAM PROPERTY

The Woodjam property is located approximately 35 km southeast of the Mount Polley copper-gold mine. It is underlain by hornfelsed Late Triassic Nicola Group volcanic and related sedimentary rocks within the contact metamorphic aureole of the Early Jurassic Takomkane batholith; a composite, quartz-saturated calcalkaline intrusion composed of hornblende monzodiorite to hornblende-biotite monzogranite. Intrusive rocks dominate the eastern portion of the property and to the west, Miocene to Pleistocene alkali olivine flood basalt of the Chilcotin Group overlie Nicola Group volcanic rocks (Wetherup, 2000; Peters, 2005). Three zones of porphyry Cu-Au mineralization (Megabuck, Takom and Spellbound) are reported for the property (Fig 10).

The Megabuck zone (400 m by 350 m) occurs within crowded plagioclase and hornblende-plagioclase-porphyritic volcanic breccia, tuff and fine-grained reworked clastic rocks and possibly coeval intrusive rocks. Mineralization consists of an early quartz-magnetite-chalcopyrite±gold stockwork system overprinted by carbonate±chalcopyrite-pyrite veinlets and surrounded by a pyritic halo. At the centre of the zone where veinlet intensity is highest, the volcaniclastic sequence is flooded with potassium feldspar and replaced by blebs of quartz, magnetite/hematite and chalcopyrite intergrowths. Quartz veinlets and stockworks contain chalcopyrite, lesser bornite and rare pyrite. Gold values show good correlation with copper, and gold is assumed to occur as microscopic inclusions within chalcopyrite grains.

The Takom zone is located 2.5 km south of the Megabuck zone. The Spellbound zone is located 2.5 km east of the Megabuck zone. Both zones are characterized by a weak quartz-chalcopyrite stockwork developed in weak to strong epidote±tourmaline hornfelsed volcaniclastic units situated adjacent to the north-trending contact of the Takomkane batholith. Quartz-carbonate vein stockworks

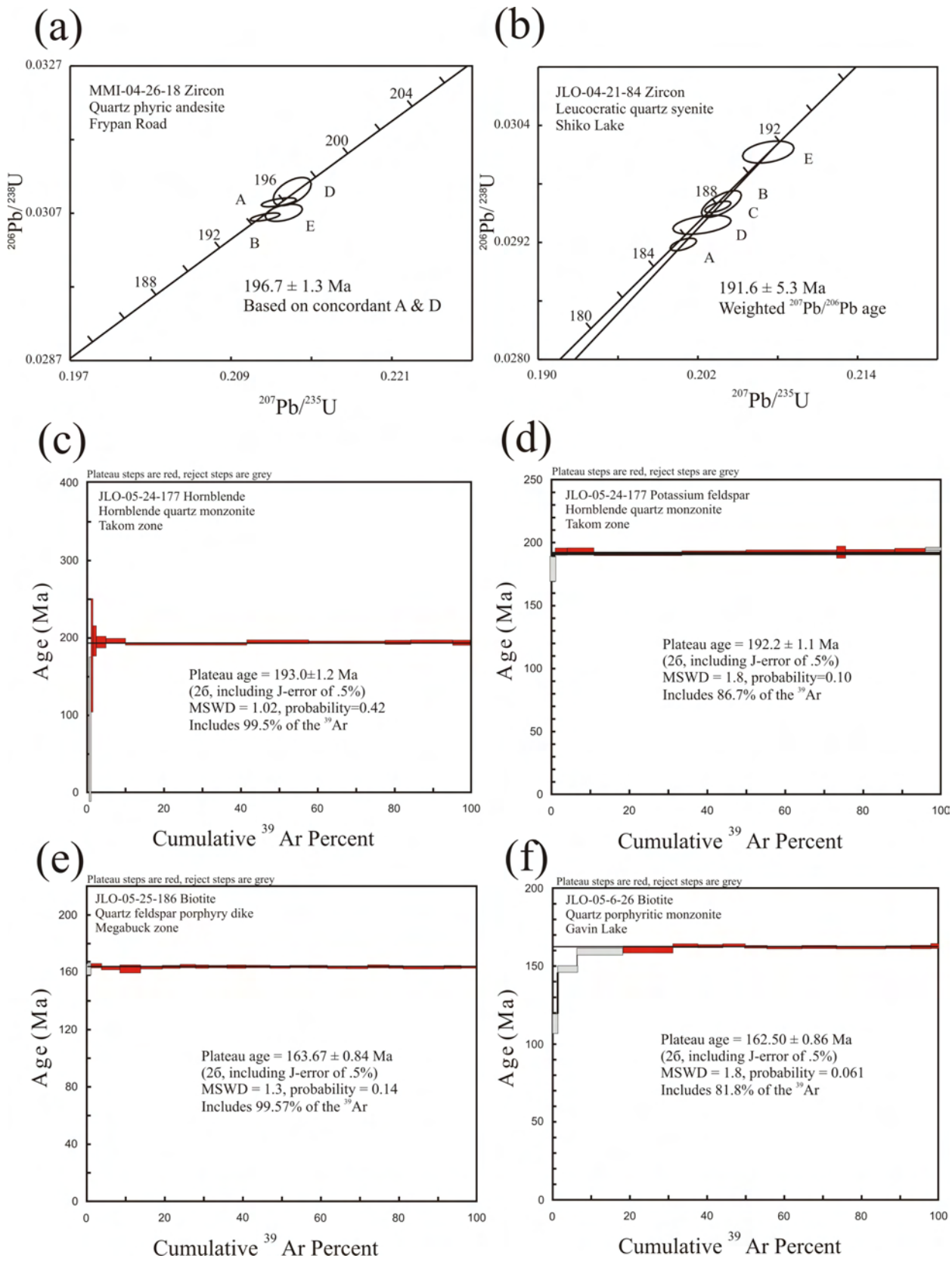

Figure 9. a) Concordia plots of U-Pb thermal ion mass spectrometry (TIMS) data for zircon samples MMI-04-26-18 from Frypan Road; A, B, C, D and E correspond to fraction numbers in Table 1; b) concordia plots of U-Pb TIMS data for zircon samples JLO-04-21-84 from Shiko Lake; A, B, C, D and E correspond to fraction numbers in Table 1; c) step-heating ^{39}Ar release plots for ^{40}Ar/^{39}Ar analyses from hornblende samples JLO-05-24-177 from the Takom zone; d) step-heating ^{39}Ar release plots for ^{40}Ar/^{39}Ar analyses for potassium feldspar samples JLO-05-24-177 from the Takom zone; e) step-heating ^{39}Ar release plots for ^{40}Ar/^{39}Ar analyses from biotite samples JLO-05-25-186 from the Megabuck zone; f) step-heating ^{39}Ar release plots for ^{40}Ar/^{39}Ar analyses for biotite samples JLO-05-6-26 from Gavin Lake. All errors are displayed as 2σ level of uncertainty.

at the Takom zone cut bleached, clay-altered pyroxene and feldspar porphyry flows and tuff where hornblende monzodiorite and quartz diorite apophyses of the Takomkane batholith intrude the sequence.

Absolute ages of the hornblende and feldspar crystal tuff, breccia and subvolcanic rocks that host mineralization on the Woodjam property were not previously known. Cannon and Pentland (1983) and Panteleyev *et al.* (1996) concluded that they are Eocene in age; Wetherup (2000), Lane (2006) and this study believe that they are Late Triassic Nicola Group – equivalent units. The tuff and volcanic breccia exhibit weak to strong epidote alteration and hornfels that increases in intensity with proximity to the Early Jurassic Takomkane batholith and supports an older Mesozoic age; however, podiform epidote replacements, potassium feldspar and tourmaline, sericite, pyrite, quartz

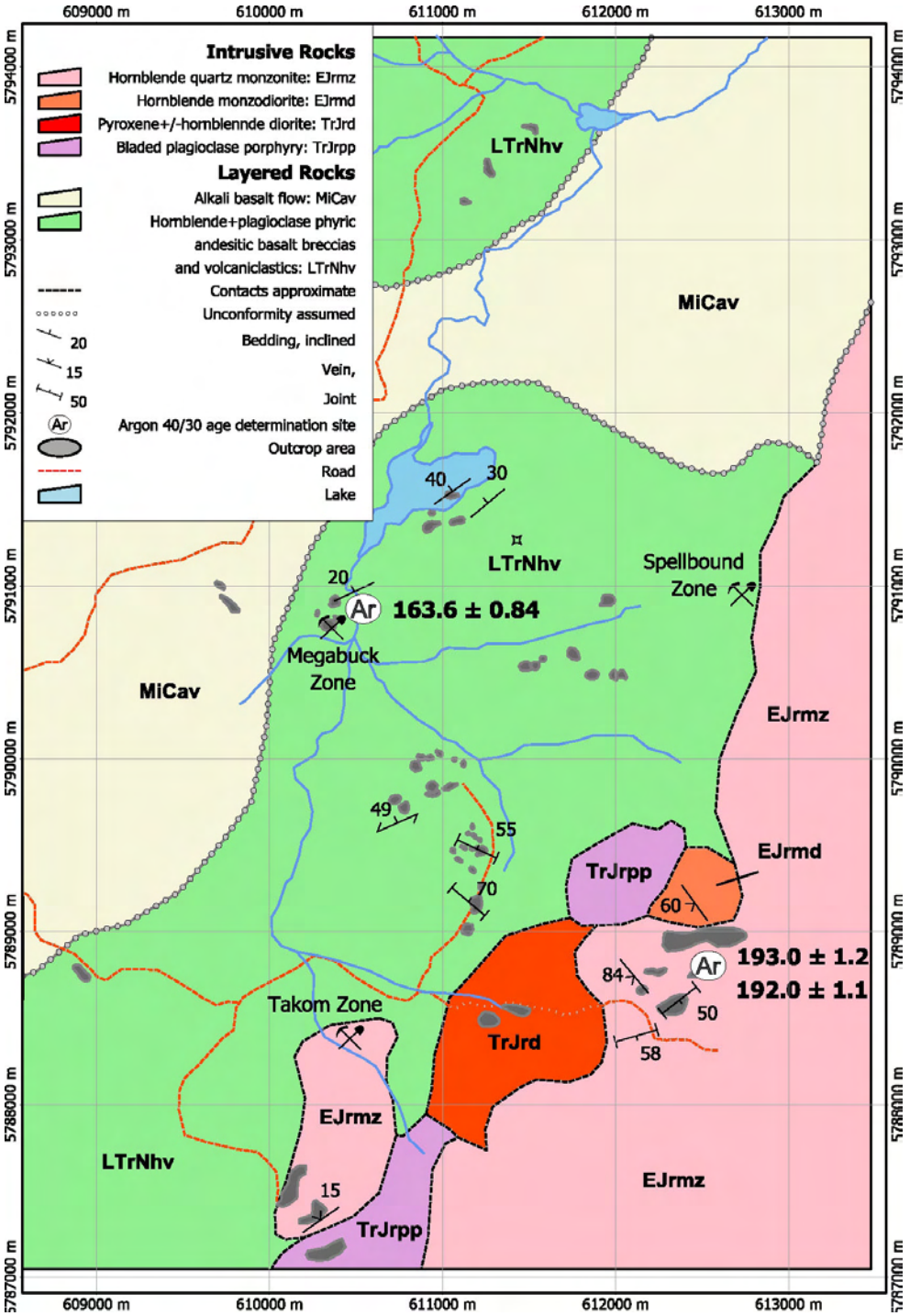

Figure 10. Compilation map of the Woodjam property showing the locations of $^{40}Ar/^{39}Ar$ isotopic age determination sites and analytical results. Incorporates unpublished assessment work by Wetherup (2000).

stockwork alteration affects both the Early Jurassic intrusion and host country rocks, and could be related to a younger event. Analogy with the Mount Polley Mine has been suggested, but the Quesnel belt alkaline Cu-Au porphyry is typically quartz undersaturated, not characterized by quartz stockwork, and they are Late Triassic in age. A better analogy might be the mineralization at the Mount Milligan deposit. It comprises four zones situated within and adjacent to the west-dipping Early Jurassic MBX stock (Sketchley *et al*., 1995). East of the stock, in the footwall, is the copper-gold MBX, which to the south passes into the gold-rich, copper-poor 66 zone. To the west, in the hangingwall of the stock, are the WBX and DWBX zones, where chalcopyrite and gold mineralization is associated with quartz veins. Woodjam mineralization is most similar to the WBX and DWBX zones.

To better understand the relationships between the silica-rich hydrothermal mineral system at the Megabuck zone and the Takomkane batholith, $^{40}Ar/^{39}Ar$ age dating was undertaken. Two samples were collected: one from the main phase of the Takomkane batholith and the other from a post-mineralization quartz-feldspar porphyry (QFP) dike that cuts Cu-Au mineralization at the Megabuck zone.

Hornblende Quartz Monzonite (05JLO-24-177)

A medium to coarse-grained equigranular hornblende±biotite quartz monzonite comprises the main phase of the Takomkane batholith, where it crops out along the eastern side of the Woodjam property. The batholith contact trends north-northeast and is characterized by a mixed border phase that includes hornblende quartz diorite, pyroxene monzodiorite and distinctive bladed feldspar porphyry (Wetherup, 2000). Regional aeromagnetic patterns suggest that the batholith border may underlie the hornblende-plagioclase porphyritic breccia, tuff and volcaniclastic rocks on the western portion of the Woodjam property.

A sample was collected from the main medium-grained, equigranular quartz monzonite exposed approximately 1 km east of the Takom zone (Fig 10). The monzonite is massive, homogeneous and unaltered. Locally, it contains ovoid epidote+plagioclase+tourmaline nodules (1–2 cm) or is cut by centimetre-wide potassium feldspar veins. Both of these features were avoided during sample collection. The collected sample contains hornblende (8–10%, 1–1.3 cm), biotite (1%, 1–2 mm), feldspar (3–6 mm) and subrounded quartz (19%) with accessory amounts of tourmaline, magnetite, apatite, epidote and pyrite.

Hornblende and potassium feldspar were separated from the quartz monzonite and analyzed separately to constrain the cooling history of the unit (Fig 9c, d). The age for the hornblende separate gave 193.0 ±1.2 Ma, with only minor Ar loss displayed in the earliest heating step. The plateau age includes 99.59% of the ^{39}Ar and provides a good undisturbed cooling age that is interpreted as the crystallization age. Potassium feldspar from this same sample gave a well-defined Ar/Ar plateau age of 192.2 ±1.1 Ma, represented by 86.7% of the ^{39}Ar. This is essentially identical within error; hornblende and potassium feldspar plateau ages for this sample support an undisturbed cooling age of *ca.* 193 Ma.

Quartz-Feldspar Porphyry Dike (05JLO-25-186)

A quartz-feldspar porphyry dike intrudes hornblende-phyric metavolcanic rocks at the Megabuck showing on the Woodjam property. The dike was intersected over a 12 m interval near the bottom of diamond drillhole WJ04-37. The dike contains stubby white plagioclase laths (40%, 3 mm), light grey quartz eyes (up to 5% and 5 mm diameter) and biotite (<1%, fresh 2–3 mm booklets), in a fine-grained altered matrix of quartz, plagioclase and potassium feldspar. Five 2 m assay samples collected across the dike returned mean values of 0.001% Cu and 0.01 g/t Au (Peters, 2005). The dike is unmineralized and is assumed to post-date mineralization. The footwall contact to the dike is faulted, and below this fault, some of the better copper and gold grades were encountered (2.05 m of 0.496% Cu and 0.205 g/t Au, and 1.74 m of 1.805% Cu and 2.204 g/t Au; Peters, 2005).

Biotite was separated from the QFP dike and analyzed to constrain the age of mineralization. Although the dike is friable and the groundmass is altered to pale, chalky clay minerals, the euhedral biotite phenocrysts are very fresh. The biotite returned an age of 163.67 ±0.84 Ma, with only minor Ar loss displayed in the earliest two heating steps (Fig 9e). The plateau age includes 99.57% of the ^{39}Ar and provides a good undisturbed cooling age for the quartz-feldspar porphyry dike that crosscuts host volcanic rocks and mineralization at the Megabuck zone.

GAVIN LAKE

The western portion of the Quesnel belt at this latitude is well defined by the north-northwest-trending edge of the Mount Polley aeromagnetic anomaly. Volcanic rocks in the belt are intruded by metre to decimetre-wide quartz porphyritic monzogranite dikes (Fig 5). The dikes consist of a fine-grained leucocratic matrix, variable amounts of finely disseminated pyrite and up to 10% euhedral quartz phenocrysts. Biotite, to several percent, and rare hornblende is present, but both are commonly completely replaced by sericite and carbonate. Weathering produces a distinctive limonitic, pinkish, fine-grained massive rock with conspicuous (2–8 mm) quartz phenocrysts. The largest concentration of these intrusive rocks occur at Gavin Lake, where a coalescing swarm of east-trending dikes and small quartz monzonite porphyry plugs intrude volcanic sedimentary rocks in an area approximately 1 km by 4 km immediately north of the lake (Logan and Bath, 2005). Sparse chalcopyrite and molybdenite mineralization is associated with quartz and potassium feldspar stockwork veining in the dikes. A similar swarm of carbonate-altered quartz-eye porphyritic monzogranite intrusions crop out along the Quesnel River, 80 km northwest of Gavin Lake, at the Kate showing. There, Cu, Au and Mo mineralization occupies narrow quartz and quartz-carbonate stockwork veinlets in the monzogranite. Pyrite dominates, with less abundant chalcopyrite, and assays return a distinctive metal assemblage elevated in bismuth, antimony, arsenic and silver values. Bailey (1978) and Panteleyev *et al*. (1996) correlate these quartz-bearing calcalkaline intrusions with hornblende-biotite monzogranite of the Nyland Lake stock and include them in the Cretaceous, Naver plutonic suite (Woodsworth *et al.,* 1991).

Quartz-Plagioclase-Porphyritic Monzogranite (05JLO-06-26)

A sample of least-altered, porphyritic quartz-plagioclase monzogranite was collected from an exploration trench located north of the east end of Gavin Lake. The rock has conspicuous euhedral plagioclase (25%, 2–3 mm), subhedral to rounded vitreous quartz phenocrysts (10%, 2–6 mm) and fresh euhedral black books of biotite (3–4%, 1 mm) in a fine-grained groundmass (55–60%) of potassium feldspar, plagioclase, quartz and opaque minerals. It is cut by narrow (0.5–1 cm wide) sheeted quartz veins mineralized with variable amounts of pyrite and chalcopyrite.

Igneous biotite was separated from the porphyritic monzogranite and analyzed to constrain the cooling history for this calcalkaline episode of magmatism and provide a minimum age for alteration and mineralization. Steps 4 through 14 of the ^{39}Ar release spectrum represent 81.4% of the total ^{39}Ar and yield a plateau age of 162.5 ±0.86 Ma. Minor Ar loss is displayed in the earliest low-temperature heating steps (Fig 9f). The plateau age is slightly too old due to the presence of excess argon. An inverse isochron plot, based on 11 points, yielded a correlation age of 161.77 ±0.99 Ma (mean standard weighted deviate = 1.13), which agrees within error with the calculated plateau age. The integrated (or total gas) age of 160.46 ±0.53 Ma is also similar to the correlation age because the sample is so highly radiogenic that the excess argon makes little difference to the calculated age.

Quartz-Plagioclase-Porphyritic Monzogranite (05JLO-06-27)

A 20 kg sample of quartz-plagioclase-porphyritic monzogranite was collected from an outcrop located north of the Gavin Lake Road, midway along the length of Gavin Lake. Zircons are clear to slightly cloudy, subhedral (slightly rounded and resorbed) prisms with cores that are evident in plane light. Cathodoluminescence (CL) imaging reveals that most grains are dominated by cores with relatively narrow rims. Some grains feature irregularly shaped rims that extend well into the interior, indicating that significant resorption occurred during magmatism (Fig 11b). Uranium-lead TIMS results for seven multigrain fractions and single grains that lie between about 185 Ma and 260 Ma are interpreted as mixtures of rim and core material or for the older grains, possibly a record of the age of the core. It is likely that for these latter grains, the narrow cores may have been completely removed during air abrasion. The youngest TIMS result at *ca.* 187 Ma is considered as a maximum age constraint (Fig 11a).

Laser ablation ICP-MS U-Pb dating was undertaken in order to better isolate the ages of cores and rims. The data are listed in Table 2. Figure 11c is a concordia plot of the laser ablation U-Pb data, highlighting the difference between core and rim ages. Cores are mainly *ca*. 200 to 240 Ma and rims are *ca*. 160 Ma. A composite rim age of 160.0 ±2.3 Ma, based on a weighted average of eight ^{206}Pb/^{238}U dates (Fig 11d), is thought to record a minimum crystallization age for the intrusion. At the 2σ level of uncertainty, this date is statistically equivalent to the biotite Ar/Ar date of 162.5 ±0.9 Ma.

INTERPRETATION AND DISCUSSION

Geochronological results from the Iron Mask batholith and Mount Polley studies corroborate earlier work and also provide new age constraints on the limits of alkaline and calcalkaline-related porphyry mineralization in the central Quesnel Terrane. Applied regionally, these results help clarify the Mesozoic metallogenic evolution of this part of the Quesnel Terrane (52.5°N). Geochronological results from this study are summarized in Table 3.

Mineral exploration and property assessment are assisted by deposit models. The recognition of the most appropriate deposit model and, in the case of BC alkaline Cu-Au porphyry deposits, the correct magmatic suite, is important for the early stage of deposit evaluation. The recognition of alkaline versus calcalkaline alteration and mineral zonation patterns are important steps to the evaluation of nascent mineral exploration targets. This is particularly true in areas with limited exposure, like many parts of the Intermontane Belt.

Iron Mask Batholith

The ages reported here for plutonic rocks and hydrothermal titanite from the Iron Mask batholith include the first cooling ages obtained for the Sugarloaf diorite. They support the stratigraphy proposed by Snyder (1994) and Snyder and Russell (1995). The U-Pb crystallization ages for samples of the Pothook, Hybrid and Cherry Creek phases of the Iron Mask batholith (Mortensen *et al.,* 1995) fall within the age range of 204 ±3 Ma. The Sugarloaf diorite is the youngest phase (from crosscutting relationships) but eludes U-Pb techniques due to low zircon content. The ^{40}Ar/^{39}Ar cooling age determinations for hornblende from two samples of Sugarloaf diorite give ages of 200.1 ±2.5 Ma and 196.3 ±1.3 Ma. The young ^{40}Ar/^{39}Ar ages for the Sugarloaf diorite are consistent with, and overlap the error envelope of the titanite cooling age for the Ajax hydrothermal assemblage. Mineralization at both the Rainbow and Gold zones is hosted by Sugarloaf hybrid units and altered hornblende porphyry phases of Sugarloaf diorite, and are likely related to late-stage fluids generated from these same phases.

Magmatic foliation in the hybrid phase is consistently oriented ~280°, suggesting tectonic control on the emplacement and cooling of the Iron Mask batholith. The timing of deformation is further constrained by a single 206.9 ±2.2 Ma cooling age for lineated pegmatitic hornblende segregations (MMI-04-4-1a) of hybrid rocks from north of Jacko Lake. The cooling age is older, but within error of the crystallization age (204.6 ±2.6 Ma) reported by Mortensen *et al*. (1995) for the hybrid phase. Schistosity is well developed within carbonate porphyroblastic augite tuff and sericitic metasediment near the south rim of the Ajax West Pit. There, Sugarloaf dike rocks are also weakly foliated. Sericite from a foliated augite tuff (JLO-04-2-17a) yielded a complex spectra with a plateau age of 205.6 ±1.3 Ma, coeval within error with hornblende having a preferred orientation within the Hybrid phase, but predates the cooling/crystallization ages of the two Sugarloaf diorite samples (JLO-04-6-67 and MMI-04-1-6). The age spectra also contain evidence for a younger (*ca*. 189 Ma) cooling event in the high-temperature steps, probably reflecting known regional Early Jurassic magmatism.

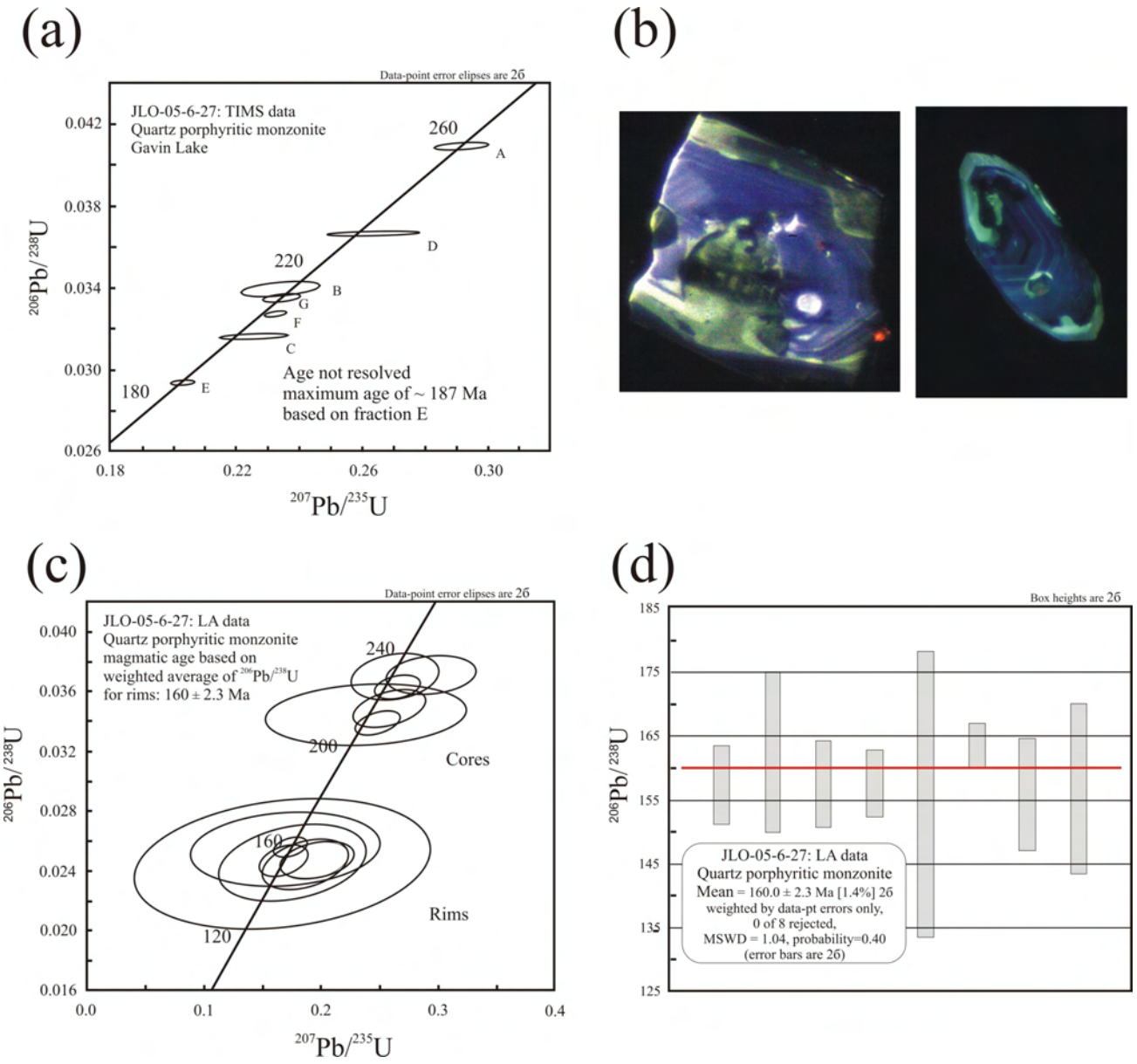

Figure 11. U-Pb concordia plots for thermal ionization mass spectrometry (TIMS); a) and laser ablation; A, B, C, D, E, F and G correspond to 7 multigrain fractions in Table 1; b) two cathodoluminescence images of single zircon grains show complex core–rim geometry and fine-scale igneous zoning in their cores. Dark lines are laser tracks across greenish rim (right image) and blue core material (right side of left image). The length of the crystals is ~0.2 mm; c) U-Pb concordia plots for TIMS data for zircon fractions from Gavin Lake porphyritic quartz monzonite; d) crystallization age based on a weighted average of eight $^{206}Pb/^{238}U$ dates from laser ablation data of zircon rims. All errors are displayed at the 2σ level of uncertainty.

The crystallization age of 198.5 ±4.5 Ma for hydrothermal titanite is assumed to represent the age of vein mineralization hosted in the Iron Mask Hybrid unit. The geometry of the vein and *en échelon* tension gash system is consistent with tops-to-the-southeast sense of motion at the time of mineralization. The 104.6 ±0.67 Ma $^{40}Ar/^{39}Ar$ cooling age for potassium feldspar separate from the vein suggests that the system was susceptible to a low-temperature thermal overprint until the mid-Cretaceous.

Mount Polley Area

The U-Pb and $^{40}Ar/^{39}Ar$ ages reported here are similar within error to previously published crystallization and cooling ages for intrusive rocks and alteration assemblages in the central Quesnel belt (Bailey, 1988, 1990; Panteleyev, 1986, 1987; Mortensen *et al.,* 1995; Panteleyev *et al.,* 1996). Geochronological data for plagioclase porphyry, pyroxene monzonite, potassium megacrystic syenite and

TABLE 3. SUMMARY OF U-PB AND $^{40}AR/^{39}AR$ ANALYSES.

Sample no	Location	Unit[a]	Method	Mineral[b]	Age ±2σ error (Ma)	Age interpretation
Iron Mask						
MMI-04-4-1a	Jacko Lake	Hybrid - pegmatitic	Ar/Ar	HRNBLD	206.9 ±2.2	Plateau age taken as crystallization age
JLO-04-2-17a	Ajax W, S wall	Foliated augite tuff	Ar/Ar	SERICITE	205.6 ±1.3	Complex plateau, Ar recoil effects
JLO-04-6-67	Sugarloaf Hill	Sugarloaf diortite	Ar/Ar	HRNBLD	200.1 ±2.5	Plateau age taken as crystallization age
MMI-04-1-6	Au zone	Sugarloaf diortite	Ar/Ar	HRNBLD	196.3 ±1.3	Plateau age taken as crystallization age
JLO-04-2-14	Ajax W, N wall	Mineralized vein	Ar/Ar	KSPAR	104.6 ±0.67	Plateau age taken as crystallization age
JLO-04-2-14	Ajax W, N wall	Mineralized vein	U/Pb	TITANITE	198.5 ±4.5	3 concordant, overlaping fractions taken as crystallization age
Mount Polley						
JLO04-24-111	Satellite stock	Pyroxene monzonite	U/Pb	ZIRCON	203.1 +1.6/-12.7	Lower intercept age of 5 point regression
JLO04-20-70b	N Bell pit	Pyroxene monzonite	Ar/Ar	HRNBLD	165.2 ±1.8	Possible pyroxene contamination & Ar recoil
JLO04-50-510	Bell pit	Kspar megacrystic monz	U/Pb	ZIRCON	205.01 ±0.3	Combined errors on three concordant fractions
MMI04-24-1	Cariboo	Hydrothermal alteration	Ar/Ar	BIOTITE	220.8 ±1.3	Plateau age taken as crystallization age
WB-05-209	NE zone	Hydrothermal alteration	Ar/Ar	BIOTITE	205.2 ±1.2	Plateau age taken as crystallization age
WB-05-209	NE zone	Hydrothermal alteration	Ar/Ar	KSPAR	130.7 ±1.0	Complex plateau, contamination or excess Ar
MMI04-26-18	Fry Pan Road	Quartz-phyric andesite	U/Pb	ZIRCON	196.7 ±1.3	Crystallization age based on two concordant fractions as crystallization age
JLO04-21-84	Shiko Lake	Quartz syenite	U/Pb	ZIRCON	191.6 ±5.3	Weighted mean $^{207}Pb/^{206}Pb$ age, minor Pb loss
JLO 24-177	Takome zone	Hornblende quartz monz	Ar/Ar	HRNBLD	193.0 ±1.2	Plateau age taken as crystallization age
JLO 24-177	Takome zone	Hornblende quartz monz	Ar/Ar	KSPAR	192.2 ±1.1	Plateau age taken as crystallization age
JLO 25-186	Megabuck zone	Quartz-feldspar porphyry	Ar/Ar	BIOTITE	163.6 ±0.84	Plateau age taken as crystallization age
JLO 6-26	Gavin Lk	Quartz phyric monz	Ar/Ar	BIOTITE	162.5 ±0.86	Plateau age taken as crystallization age
JLO 6-27	Gavin Lk	Quartz phyric monz	U/Pb	ZIRCON	160.0 ±2.3	Weighted average $^{206}Pb/^{238}U$ age for rims taken as crystallization age

[a] Kspar, potassium feldspar; monz, monzonite

[b] KSPAR, potassium feldspar; HRNBLD, hornblende

diorite phases of the Mount Polley intrusive complex range between 204.7 ±3 Ma (Mortensen *et al*., 1995; this study) and *ca*. 197 Ma. The youngest *ca*. 197 Ma age limit is defined by quartz-phyric andesite tuff that apparently overlaps the mineralized Mount Polley Igneous Complex (MPIC) and was deposited following local emergence and incision of the arc. Quartz-bearing andesite tuff, volcanic conglomerate and interbedded hornblende-phyric volcaniclastic rocks unconformably (?) overlie the MPIC north of Polley Lake Road. The sequence is unmineralized and characterized by low-temperature white and pink zeolite assemblages but not potassic, albitic or calcsilicate hypogene alteration assemblages. Stratigraphic and petrographic relationships support an extrusive origin for the tuff and a change from quartz-undersaturated to quartz-saturated magmatism and isolated volcanism.

In this study, $^{40}Ar/^{39}Ar$ age determinations for biotite associated with chalcopyrite mineralization from the Northeast zone (Wight Pit) gave a date of 205.2 ±1.2 Ma, which we regard as the age of mineralization. This age is indistinguishable from the U-Pb crystallization age of a potassium feldspar megacrystic dike in the Bell pit (205.01 ±0.3 Ma) and consistent with high-level emplacement and rapid cooling of the intrusive complex. Map relations in the pits and drillcore show that alteration and brecciation followed the intrusion of the megacrystic dike phase because fragments of this unit are present in the Northeast zone breccia. Mineralization postdates breccia formation that was restricted to a single, main event, due to the paucity of clasts of breccia within breccia zones. Northeast zone copper mineralization, however, appears to have been introduced in two stages. First-stage chalcopyrite, as an interconnected network of fractures and veinlets, is overprinted by later bornite, rimming and replacing chalcopyrite, and focused in steep northwest-trending centimetre-thick sheeted veins.

Pervasive potassic alteration precedes breccia formation and mineralization at Mount Polley; therefore, the 130.7 ±1.0 Ma potassium feldspar plateau age for WB-05-209 must reflect a much younger, probably local, thermal overprint. Young, low-temperature (*i.e.,* below the Ar closure temperature for biotite, 300–350°C) hydrothermal event(s) could reset the *ca.* 205 Ma mineralizing event in the potassium feldspar. Plutonic potassium feldspar has Ar closure temperatures of 200 to 225°C (Foland, 1994) or as low as 150°C (McDougall and Harrison, 1999). Evidence for a *ca.* 130 Ma magmatic or thermal event in this part of the Quesnel belt has not been previously documented, although Mortimer *et al*. (1990) report a 130 Ma date from lamprophyre dikes that crosscut Quesnel Terrane Nicola Group rocks east of Kamloops.

Biotite cooling ages (below 350°C) for the MPIC include the 205.2 ±1.2 Ma plateau age from the Northeast zone (WB-5-209) and the 220.8 ±1.3 Ma plateau age from coarse hydrothermal alteration assemblages associated with hypogene mineralization in the Cariboo pit (MMI-04-24-1). The relatively undisturbed age spectrum for biotite associated with hypogene mineralization in the Northeast zone contrasts sharply with the biotite cooling ages from the Cariboo pit. The biotite plateau age for Cariboo pit sample MMI-04-24-1 predates crystallization ages of the MPIC rocks by approximately 15 Ma. We believe this age to be erroneous. Cooling ages calculated for hornblende (203.1 ±2.0 Ma) and titanite (200.7 ±2.8 Ma) from the Bootjack stock (Bailey and Archibald, 1990; Mortensen *et al.,* 1995) indicate variable but considerably slower cooling (below 600–550°C) for this intrusion (*i.e*., younger ages for minerals with higher closure temperatures).

Satellite plugs of pyroxene monzonite crop out peripheral to the MPIC. Sample JLO-04-24-111 has a U-Pb zircon crystallization age of 203.1 +1.6/–12.7 Ma, which overlaps within error the U-Pb zircon crystallization age range of the

MPIC. Sample JLO-04-20-70b is mineralogically identical to other Late Triassic pyroxene monzonite, but has a Middle Jurassic $^{40}Ar/^{39}Ar$ plateau age (165.2 ±1.8 Ma). This age is interpreted to reflect a Middle Jurassic thermal overprint and is complicated by excess argon and recoil related to contamination. Petrographic analysis of this sample shows that the hornblende is chloritic and makes up a much smaller component of the monzonite than initially assumed, thus, it is probable that the hornblende separated for $^{40}Ar/^{39}Ar$ dating included a significant proportion of pyroxene.

The leucocratic quartz syenite that cuts monzodiorite and trachytic feldspar porphyry syenite of the Shiko Lake stock has a U-Pb zircon crystallization age of 191.6 ±5.3 Ma. This provides a minimum age for copper-gold mineralization that is hosted in all three units. It is possible, however, that the intrusion of the younger quartz-bearing syenite incorporated and remobilized earlier mineralization associated with the quartz-undersaturated monzodiorite and porphyritic syenite phases. Mineral assemblages in these earlier alkaline phases (actinolite, potassium feldspar, magnetite, pyrite and chalcopyrite) are similar to those in the Cariboo pit at Mount Polley.

Copper and gold quartz stockwork mineralization at the Woodjam property is hosted in epidote-magnetite-pyrite±tourmaline hornfelsed hornblende-plagioclase-phyric andesitic breccia, bedded volcaniclastic rocks and apophyses of the Takomkane batholith. The Takomkane is a complex batholith that apparently spans the Late Triassic to Early Jurassic boundary (*ca*. 202–193 Ma; Schiarizza and Macauley, 2007), the main phase in the vicinity of the Woodjam property is Early Jurassic (193 Ma). An unmineralized quartz-feldspar-biotite porphyry dike that crosscuts mineralization at the Megabuck zone is herein dated as 163 Ma, providing a minimum age constraint on mineralization (*i.e.,* not Tertiary as previously proposed). The quartz stockwork style of Cu-Au mineralization at the Megabuck is dissimilar to the Late Triassic alkaline centres in the area (*i.e.*, Mount Polley, Shiko Lake and QR) and cuts an Early Jurassic hornfels related to the Takomkane batholith. We interpret the age of the mineralization at the Woodjam property to be Early Jurassic, *ca.* 193 Ma. It is similar in style to *ca.*183 Ma mineralization at Mount Milligan, ~275 km to the northwest.

Copper and molybdenum quartz stockwork mineralization at Gavin Lake is associated with a quartz-phyric calcalkaline dike swarm. Geochronology indicates Middle to Late Triassic xenocrystic zircons mantled by Middle Jurassic zircon rims that give concordant ages of *ca.*160.0 Ma and are interpreted as the age of intrusion. The xenocrystic zircons have originated from either the source region or the wallrocks in the path of ascent, and possess no evidence for any extensive interaction with older North American crust. Regional correlative stocks and dikes are characteristically iron-carbonate altered, pyritic high-level siliceous leucogranite intrusions.

CONCLUSIONS

Magmatic, tectonic and geochronological features of the Iron Mask and Mount Polley areas support the following conclusions:

- intrusion of the main phases of these alkaline intrusive complexes occurred over a short time span in the Late Triassic (204 ±3 Ma)
- probably in a shallow or subvolcanic environment
- mineralization was focused over a relatively short time interval(s) from 205 to 200 Ma at the Triassic–Jurassic boundary (Woodjam is calcalkaline type and Early Jurassic in age)
- ductile deformation accompanied the intrusion and cooling of the early phases of the Iron Mask batholith

ACKNOWLEDGMENTS

This work was made possible through the financial support of our corporate partners, Abacus Mining and Exploration Corporation and Imperial Metals Corporation. Geochronological sample analyses were conducted in partnership with the Pacific Centre for Isotopic and Geochemical Research at the Department of Earth and Ocean Sciences, The University of British Columbia. We thank Brian Grant and Paul Schiarizza for their careful review of the manuscript.

REFERENCES

Abacus Mining and Exploration Corporation (2006): Afton Area Properties – Rainbow and DM/Audra/Crescent Resource Summary; *Abacus Mining and Exploration Corporation*, Press release, July 6, 2006, URL <http://www.amemining.com/s/NewsReleases.asp?ReportID=111406&_Type=News-Releases&_Title=Afton-Area-Properties-Rainbow-and-DMAudraCrescent-Resource-Summary> [December 2006].

Ash, C.H., Reynolds, P.H., Creaser, R.A. and Mihalynuk, M.G. (2007): ^{40}Ar-^{39}Ar and Re-O isotopic ages for hydrothermal alteration and related mineralization in the Highland Valley Cu-Mo deposit, SW BC; *in* Geological Fieldwork 2006, *BC Ministry of Energy, Mines and Petroleum Resources*, Paper 2007-1 and *Geoscience BC*, Report 2007-1, pages 19–24.

Bailey, D.G. (1978): The Geology of the Morehead Lake Area; unpublished PhD thesis, *Queen's University*, 198 pages.

Bailey, D.G. (1988): Geology of the Hydraulic Map Area, NTS 93A/12; *BC Ministry of Energy, Mines and Petroleum Resources,* Preliminary Map 67, scale 1:50 000.

Bailey, D.G. (1990): Geology of the Central Quesnel Belt, British Columbia; *BC Ministry of Energy, Mines and Petroleum Resources*, Open File 1990-31, 1:100 000 map with accompanying notes.

Bailey, D.G. and Archibald, D.A. (1990): Age of the Bootjack Stock, Quesnel Terrane, south-central British Columbia (93A); *in* Geological Fieldwork 1989, *BC Ministry of Energy, Mines and Petroleum Resources*, Paper 1990-1, pages 79–82.

Bailey, D.G. and Hodgson, C.J. (1979): Transported altered wall rock in laharic breccias at the Cariboo-Bell Cu-Au porphyry deposit, British Columbia; *Economic Geology*, Volume 74, pages 125–128.

Barr, D.A., Fox, P.E., Northcote, K.E. and Preto, V.A. (1976): The Alkaline Suite Porphyry Deposits: A Summary; *in* Porphyry Deposits of the Canadian Cordillera, Sutherland Brown, A., Editor, *Canadian Institute of Mining and Metallurgy*, Special Volume 15, pages 359–367.

Bath, A.B. and Logan, J.M. (2006): Petrography and geochemistry of the Late Triassic Bootjack Stock, south-central British

Columbia; *in* Geological Fieldwork 2005, *BC Ministry of Energy, Mines and Petroleum Resources*, Paper 2006-1.

Breitsprecher, K. and Mortensen, J.K. (2004): BC Age 2004A-1: A database of isotopic age determinations for rock units from British Columbia; *BC Ministry of Energy, Mines and Petroleum Resource,* Open File 2004-03.

Campbell, R.B. (1978): Quesnel Lake (93A) map-area; *Geological Survey of Canada*, Open File Map 574.

Cannon, R. and Pentland, W.S. (1983): A geological, geophysical and geochemical report on the Horsefly property; *BC Ministry of Energy, Mines and Petroleum Resources,* AR11379.

Cockfield, W.E. (1948): Geology and mineral deposits of Nicola map area, British Columbia; *Geological Survey of Canada*, Memoir 249, 164 pages.

Evans, G. (1992): Property geology map covering the northwest margin of the Iron Mask Batholith in the vicinity of the Pothook pit; *Teck Exploration Ltd*, unpublished 1:2500 map.

Foland, K. A. (1994): Argon diffusion in feldspars; *in* Feldspars and Their Reactions, Parsons, I., Editor, *Kluwer*, pages 415–447.

Fraser, T.M. (1994): Hydrothermal breccias and associated alteration of the Mount Polley copper-gold deposit; *in* Geological Fieldwork 1993, *BC Ministry of Energy, Mines and Petroleum Resources*, Paper 1994-1, pages 259–267.

Fraser, T.M. (1995): Geology, Alteration and the Origin of Hydrothermal Breccias at the Mount Polley Alkalic Porphyry Copper-Gold Deposit, South-Central British Columbia; unpublished MSc thesis, *The University of British Columbia*, 259 pages.

Fraser, T.M., Stanley, C.R., Nikic, Z.T., Pesalj, R. and Gorc, D. (1995): The Mount Polley Copper-Gold Alkalic Porphyry Deposit, South-Central British Columbia; *in* Porphyry Deposits of the Northern Cordillera, Schroeter, T.G., Editor, *Canadian Institute of Mining and Metallurgy*, Special Volume 46, pages 609–622.

Ghent, E.D., Erdmer, P., Archibald, D.A. and Stout, M.Z. (1996): Pressure-temperature and tectonic evolution of Triassic lawsonite – aragonite blueschists from Pinchi Lake, British Columbia; *Canadian Journal of Earth Sciences*, Volume 33, pages 800–810.

Harrison, T.M. (1981): Diffusion of ^{40}Ar in hornblende; *Contributions to Mineralogy and Petrology,* Volume 78, pages 324–331.

Hodgson, C.J., Bailes, R.J. and Versoza, R.S. (1976): Cariboo-Bell; *in* Porphyry Deposits of the Canadian Cordillera, Sutherland Brown, A., Editor, *Canadian Institute of Mining and Metallurgy*, Special Volume 15, pages 388–396.

Krogh, T.E. (1982): Improved accuracy of U-Pb ages by the creation of more concordant systems using an air abrasion technique; *Geochimica et Cosmochimica Acta*, Volume 46, pages 637–649.

Kwong, Y.T.J. (1987): Evolution of the Iron Mask batholith and its associated copper mineralization; *BC Ministry of Energy, Mines and Petroleum Resources*, Bulletin 77, 55 pages.

Lane, B. (2006): Central Region; *in* Exploration and Mining in British Columbia 2005, *BC Ministry of Energy, Mines and Petroleum Resources,* pages 41–52.

Lang, J.R. and Stanley, C.R. (1995): Contrasting styles of alkalic porphyry copper-gold deposits in the northern Iron Mask batholith, Kamloops, British Columbia; *in* Porphyry Deposits of the Northwestern Cordillera of North America, Schroeter, T.G., Editor, *Canadian Institute of Mining, Metallurgy and Petroleum*, Special Volume 46.

Lang, J.R., Lueck, B., Mortensen, J.K., Russell, J.K., Stanley, C.R. and Thompson, J.F.H. (1995): Triassic-Jurassic silica-undersaturated and silica-saturated intrusions in the Cordillera of British Columbia: implications for arc magmatism; *Geology*, Volume 23, pages 451–454.

Logan, J.M. and Bath, A.B. (2006): Geochemistry of Nicola Group basalt from the central Quesnel trough at the latitude of Mount Polley (NTS 093A/5, 6, 11, 12), central British Columbia; *in* Geological Fieldwork 2005, *BC Ministry of Energy, Mines and Petroleum Resources*, Paper 2006-1, pages 83–98.

Logan, J.M. and Mihalynuk, M.G. (2005a): Regional geology and setting of the Cariboo, Bell, Springer and Northeast Porphyry Cu-Au zones at Mount Polley, south-central British Columbia; *in* Geological Fieldwork 2004, *BC Ministry of Energy, Mines and Petroleum Resources*, Paper 2005-1, pages 249–270.

Logan, J.M. and Mihalynuk, M.G. (2005b) Porphyry Cu-Au deposits of the Iron Mask batholith, southeastern British Columbia; *in* Geological Fieldwork 2004, *BC Ministry of Energy, Mines and Petroleum Resources*, Paper 2005-1, pages 271–290.

Logan, J.M., Mihalynuk, M.G., Ullrich, T.D. and Friedman, R. (2006): Geology of the Iron Mask Batholith; *BC Ministry of Energy, Mines and Petroleum Resources*, Open File Map 2006-11.

Logan, J.M., Bath, A.B., Mihalynuk, M.G., Ullrich, T.D. and Friedman, R. (2007): Regional Geology of the Mount Polley area, central British Columbia; *BC Ministry of Energy, Mines and Petroleum Resources*, Geoscience Map 2007-1.

Ludwig K.R. (2003): Isoplot 3.00, a geochronological toolkit for Microsoft Excel; *University of California at Berkeley*, Berkeley Geochronology Center, Special Publication No. 4.

Mathews, W.H. (1989): Neogene Chilcotin basalts in south-central British Columbia: geology, ages, and geomorphic history; *Canadian Journal of Earth Sciences*, Volume 26, pages 969–982.

McDougall, I. and Harrison, T.M. (1999): Geochronology and Thermochronology by the ^{40}Ar/^{39}Ar Method; *Oxford University Press*, 269 pages.

Mihalynuk, M.G., Erdmer, P., Ghent, E.D., Cordey, F., Archibald, D.A., Friedman, R.M. and Johannson, G.G. (2004): Coherent French Range blueschist: Subduction to exhumation in <2.5 m.y.?; *Geological Society of America*, Bulletin, Volume 116, No. 7/8, pages 910–922.

Mortensen, J.K., Ghosh, D.K. and Ferri, F. (1995): U-Pb geochronology of intrusive rocks associated with copper-gold porphyry deposits in the Canadian Cordillera; *in* Porphyry Deposits of the Northwestern Cordillera of North America, Schroeter, T.G., Editor, *Canadian Institute of Mining, Metallurgy and Petroleum*, Special Volume 46, pages 142–158.

Mortimer, N. (1987): The Nicola Group: Late Triassic and Early Jurassic subduction-related volcanism in British Columbia; *Canadian Journal of Earth Sciences*, Volume 24, pages 2521–2536.

Mortimer, N., van der Heyden, P., Armstrong, R.L. and Harakal, J. (1990): U-Pb and K-Ar dates related to the timing of magmatism and deformation in the Cache Creek Terrane and Quesnellia, southern British Columbia; *Canadian Journal of Earth Sciences*, Volume 27, pages 117–123.

Nixon, G.T., Archibald, D.A. and Heaman, L.M., (1993): ^{40}Ar-^{39}Ar and U-Pb geochronometry of the Polaris Alaskan-type complex, British Columbia; precise timing of Quesnellia – North America interaction; *in* Geological Association of Canada – Mineralogical Association of Canada Annual Meeting, Program with Abstracts, Joint Annual Meeting, *Geological Association of Canada*, page 76.

Northcote, K.E. (1974): Geology of the northwest half of the Iron Mask Batholith; *in* Geological Fieldwork 1974, *BC Ministry of Energy, Mines and Petroleum Resources*, Paper 1975-1, pages 22–26.

Northcote, K.E. (1977): Preliminary Map No. 26 (Iron Mask Batholith) and accompanying notes; *BC Ministry of Energy, Mines and Petroleum Resources*, 8 pages.

Oliver, J.L. (1995): Report on the 1994 exploration program Rainbow property; *BC Ministry of Energy, Mines and Petroleum Resources,* AR23917.

Palfy, J., Smith, P.L. and Mortensen, J.K. (2000): A U-Pb and ^{40}Ar-^{39}Ar time scale for the Jurassic; *Canadian Journal of Earth Sciences*, Volume 37, pages 923–944.

Panteleyev, A. (1987): Quesnel Gold belt – alkalic volcanic terrane between Horsefly and Quesnel lakes (93A/6); *in* Geological Fieldwork 1986, *BC Ministry of Energy, Mines and Petroleum Resources*, Paper 1987-1, pages 125–133.

Panteleyev, A. (1988): Quesnel mineral belt – The central volcanic axis between Horsefly and Quesnel Lakes (93A/5E, 6W); *in* Geological Fieldwork 1987, *BC Ministry of Energy, Mines and Petroleum Resources*, Paper 1988-1, pages 131–137.

Panteleyev, A. and Hancock, K.D. (1989a): Quesnel mineral belt: summary of the geology of the Beaver Creek – Horsefly River map area; *in* Geological Fieldwork 1988, *BC Ministry of Energy, Mines and Petroleum Resources*, Paper 1989-1, pages 159–166.

Panteleyev, A., Bailey, D.G., Bloodgood, M.A. and Hancock, K.D. (1996): Geology and mineral deposits of the Quesnel River–Horsefly map area, central Quesnel Trough, British Columbia (NTS 93A/5, 6, 7, 11, 12, 13; 93B/9, 16; 93G/1; 93H/4); *BC Ministry of Energy, Mines and Petroleum Resources*, Bulletin 97, 156 pages.

Parrish, R., Roddick, J.C., Loveridge, W.D. and Sullivan, R.W. (1987): Uranium lead analytical techniques at the geochronology laboratory, Geological Survey of Canada; *in* Radiogenic Age and Isotopic Studies, Report 1, *Geological Survey of Canada*, Paper 87-2, pages 3–7.

Paterson, I. and Harakal, J. (1974): Potassium-argon dating of blueschists from Pinchi Lake, central British Columbia; *Canadian Journal of Earth Sciences*, Volume 11, pages 1007–1011.

Peters, L.J. (2005): Summary technical report on the Woodjam claims, Cariboo Mining District; unpublished report, *Fjordland Exploration Inc*., 115 pages.

Preto, V.A. (1967): Geology of the eastern part of the Iron Mask Batholith; *in* BC Minister of Mines Annual Report 1967, *BC Ministry of Energy, Mines and Petroleum Resources*, pages 137–147.

Preto, V.A. (1972): Report on Afton, Pothook; *in* Geology, Exploration and Mining 1972, *BC Ministry of Energy, Mines and Petroleum Resources*, pages 209–220.

Preto, V.A. (1979): Geology of the Nicola Group between Merritt and Princeton, British Columbia; *BC Ministry of Energy, Mines and Petroleum Resources*, Bulletin 69, 90 pages.

Preto, V.A., Osatenko, M.J., McMillan, W.J. and Armstrong, R.L. (1979): Isotopic dates and strontium isotopic ratios for plutonic and volcanic rocks in the Quesnel trough and Nicola belt, south-central British Columbia; *Canadian Journal of Earth Sciences*, Volume 16, pages 1658–1672.

Renne, P.R., Swisher, C.C., III, Deino, A.L., Karner, D.B., Owens, T. and DePaolo, D.J. (1998): Intercalibration of standards, absolute ages and uncertainties in $^{40}Ar/^{39}Ar$ dating; *Chemical Geology*, Volume 145, Numbers 1–2, pages 117–152.

Roback, R.C., Sevigny, J.H. and Walker, N.W. (1994): Tectonic setting of the Slide Mountain Terrane, southern British Columbia; *Tectonics*, Volume 13, pages 1242–1258.

Roddick, J.C. (1987): Generalized numerical error analysis with application to geochronology and thermodynamics; *Geochimica et Cosmochimica Acta*, Volume 51, pages 2129–2135.

Ross, K.V. (1993): Geology of the Ajax East and West, silica-saturated, alkali copper-gold porphyry deposits, Kamloops, south-central British Columbia; unpublished MSc thesis, *The University of British Columbia*, Vancouver, 210 pages.

Ross, K.V. (2004): Alteration study of the Northeast zone, Mount Polley mine, British Columbia; unpublished report, *Imperial Metals Corporation*, 84 pages.

Ross, K.V., Godwin, C.I., Bond, L. and Dawson, K.M. (1995): Geology, alteration and mineralization in the Ajax East and Ajax West deposits, southern Iron Mask batholith, Kamloops, British Columbia; *in* Porphyry Deposits of the Northwestern Cordillera of North America, Schroeter, T.G., Editor, *Canadian Institute of Mining, Metallurgy and Petroleum*, Special Volume 46, pages 565–580.

Schiarizza, P. (1989): Structural and stratigraphic relationships between the Fennel Formation and Eagle Bay Assemblage, western Omineca Belt, south-central British Columbia: implications for Paleozoic tectonics along the paleocontinental margin of western North America; unpublished MSc thesis, *University of Calgary*, Calgary, Alberta, 343 pages.

Schiarizza, P. and Macauley, J. (2007): Geology and mineral occurrences of the Hendrix Lake area, south-central British Columbia (93A/02); *in* Geological Fieldwork 2006, *BC Ministry of Energy, Mines and Petroleum Resources*, Paper 2007-1 and *Geoscience BC*, Report 2007-1, pages 179–202.

Sketchley, D.A., Rebagliati, C.M. and Delong, C. (1995): Geology, alteration and zoning patterns of the Mt. Milligan copper-gold deposits; *in* Porphyry Deposits of the Northwestern Cordillera of North America, Schroeter, T.G., Editor, *Canadian Institute of Mining, Metallurgy and Petroleum*, Special Volume 46, pages 650–665.

Stacey, J.S. and Kramers, J.D. (1975): Approximation of terrestrial lead isotope evolution by a two-stage model; *Earth and Planetary Science Letters*, Volume 26, pages 207–221.

Snyder, L.D. (1994): Petrological studies within the Iron Mask batholith, south-central British Columbia; unpublished MSc thesis, *The University of British Columbia*, Vancouver, 192 pages.

Snyder, L.D. and Russell, J.K. (1993): Field constraints on diverse igneous processes in the Iron Mask Batholith (92L/9); *in* Geological Fieldwork 1992, *BC Ministry of Energy, Mines and Petroleum Resources*, Paper 1993-1, pages 281–286.

Snyder, L.D. and Russell, J.K. (1994): Petrology and stratigraphic setting of the Kamloops Lake picritic basalts, Quesnellia Terrane, South-central B.C.; *in* Geological Fieldwork 1993, BC Ministry of Energy, Mines and Petroleum Resources, Paper 1994-1, pages 297–309.

Snyder, L.D. and Russell, J.K. (1995): Petrogenetic relationships and assimilation processes in the alkalic Iron Mask batholith, south-central British Columbia; *in* Porphyry Deposits of the Northwestern Cordillera of North America, Schroeter, T.G., Editor, *Canadian Institute of Mining, Metallurgy and Petroleum*, Special Volume 46, pages 593–608.

Stanley, C.R. (1994): Geology of the Pothook alkalic copper-gold porphyry deposit, Afton Mining Camp, British Columbia (92I/9, 10); *in* Geological Fieldwork 1993, *BC Ministry of Energy, Mines and Petroleum Resources*, Paper 1994-1, pages 275–284.

Struik, L.C., Parrish, R.R. and Gerasimoff, M.D. (1992): Geology and age of the Naver and Ste Marie plutons, central British Columbia; *in* Radiogenic age and isotopic studies: Report 5; *Geological Survey of Canada*, Paper 91-2, pages 155–162.

Thirlwall, M.F. (2000): Inter-laboratory and other errors in Pb isotope analyses investigated using a ^{207}Pb–^{204}Pb double spike: *Chemical Geology*, Volume 163, pages 299-322.

Travers, W.B. (1977): Overturned Nicola and Ashcroft strata and their relations to the Cache Creek Group, southwestern Intermontane Belt, British Columbia; *Canadian Journal of Earth Sciences*, Volume 15, pages 99–116.

Wetherup, S. (2000): Diamond drilling report on the Woodjam Property; *BC Ministry of Energy, Mines and Petroleum Resources,* AR26242.

Woodsworth, G.J., Anderson, R.G. and Armstrong, R.L. (1991): Plutonic Regimes: Chapter 15; *in* Geology of the Cordilleran Orogen in Canada, Gabrielse, H. and Yorath, C.J., Editors, *Geological Association of Canada*, Geology of Canada, Volume 4, pages 491–531.